CROATICA CHEMICA ACTA CCACAA **75** (3) 727–767 (2002)

ISSN-0011-1643
CCA-2829

Authors' review

Factors Influencing the Stability of Low Temperature Tetragonal ZrO_2

Goran Štefanić and Svetozar Musić*

Division of Materials Chemistry, Ruđer Bošković Institute, P. O. Box 180, 10002 Zagreb, Croatia

Received November 27, 2001; revised February 18, 2002; accepted February 22, 2002

Various factors that influence the appearance of a tetragonal (*t*-) ZrO_2 polymorph at room temperature have been extensively investigated. Several proposed models emphasize the role of anionic impurities (SO_4^{2-}, OH^-), crystallite size (surface energy), structural similarities between the starting material and *t*-ZrO_2, lattice strains, water vapor, lattice defects (oxygen vacancies), *etc*. Our investigations, focused on the stability of low temperature *t*-ZrO_2, showed that, regardless of the structural differences in the starting zirconium materials, their thermal decomposition products crystallized into a metastable *t*-ZrO_2. The *t*-$ZrO_2 \rightarrow$ *m*-ZrO_2 transformation occurred during the cooling or further calcination in the presence of air at atmospheric pressure. On the other hand, if these processes are performed in vacuum, the metastable phase is preserved. These observations indicate that a metastable *t*-ZrO_2 appears at room temperature as a result of stabilization caused by introduction of oxygen vacancies, similarly as in the solid solutions with aliovalent cations. A decrease in the specific surface area of ZrO_2 grains or the presence of the substances that enter into strong surface interactions with ZrO_2 (SO_4^{2-}, Cr_2O_3) prevents the diffusion of oxygen from the atmosphere into the ZrO_2 lattice and due to this fact the metastable *t*-ZrO_2 is stabilized. On the other hand, lattice strain and grain size of metastable *t*-ZrO_2 could not be clearly related to its stability.

Key words: *t*-ZrO_2, *m*-ZrO_2, hydrous zirconia, oxygen vacancies, lattice strain, XRD, DSC.

* Author to whom correspondence should be addressed. (E-mail: stefanic@rudjer.irb.hr)

BACKGROUND

In dependence on the temperature, ZrO_2 appears in three different polymorphs: monoclinic, tetragonal and cubic. At room temperature (RT), pure zirconia is monoclinic (m-ZrO_2), having a distorted fluorite-type (CaF_2) structure, with the Zr atom in coordination seven. At high temperature the following ZrO_2 polymorph transformations occur:

$$\text{monoclinic} \xrightarrow{1170\ ^\circ\text{C}} \text{tetragonal} \xrightarrow{2370\ ^\circ\text{C}} \text{cubic} \xrightarrow{2680\ ^\circ\text{C}} \text{melt}$$

In both high-temperature phases the Zr atom assumes coordination eight, as in CaF_2, while in tetragonal form the O atom is displaced from its ideal position $\frac{1}{4}$, $\frac{1}{4}$, $\frac{1}{4}$. Because of its high melting point, zirconia is an attractive refractory material. However, the volume expansion of the tetragonal to a monoclinic transformation causes crumbling of zirconia ceramics on cooling from the sintering temperature.[1] This transformation occurred with very small shifts of atoms and could not be suppressed by rapid cooling. However, a metastable t-ZrO_2 often appeared besides m-ZrO_2 at RT.

In the thirties, Clark and Reynolds[2] detected a low temperature t-ZrO_2 in the thermal decomposition products of the $ZrOCl_2 \cdot 8H_2O$ salt. The same authors observed the presence of t-ZrO_2 in the crystallization product of hydrous zirconia, obtained upon calcination at 500 °C. The reason for the formation of this high temperature polymorph at RT is still a matter of controversy. Several proposed models are given in Table I.

TABLE I

Models of t-ZrO_2 stabilization at room temperature

Model	References
1. Influence of anionic impurities	3–9
2. Influence of particle size (surface energy)	10–14
3. Influence of lattice strains	15, 16
4. Structural similarities between precursor materials and t-ZrO_2	17–21
5. Influence of lattice defects (oxygen vacancies)	22, 23
6. Influence of water vapor	24, 25

The first mentioned mechanism of the t-ZrO_2 stabilization emphasized the influence of Cl^- anions remaining inside the crystal lattice during the thermal treatment of the starting material.[3] The stabilizing influence of

SO_4^{2-} and PO_4^{3-} anions was investigated in several papers.[4–9] Srinivasan *et al.*[5–7] concluded that the adsorption of SO_4^{2-} anion inhibits t-$ZrO_2 \rightarrow m$-ZrO_2 transformation by covering oxygen-deficient surface sites that initiate phase transformation. Garvie[10–12] suggested that the stabilization of t-ZrO_2 at RT resulted from the lower surface energy of t-ZrO_2, as compared with that of m-ZrO_2. The experimental results obtained by ball-milling under ambient conditions supported this hypothesis. When the grinding of the starting material sufficiently decreased the crystallite size, the m-$ZrO_2 \rightarrow t$-ZrO_2 transformation occurred.[13] Mitsuhashi *et al.*[15] extended the theory of Garvie[10–12] by introducing lattice strains. They found that strain-free single-domain tetragonal particles transformed much easier than polydomain particles with large strains. On the basis of radial distribution functions obtained by X-ray and neutron diffractions, Livage *et al.*[17] found that the local atomic arrangement in amorphous zirconia (Zr–Zr and Zr–O distances) was similar to that of t-ZrO_2. This result was also supported by Raman scattering.[18] Tani *et al.*[19] suggested that, under hydrothermal conditions, the t-ZrO_2 crystallized topotactically on the nuclei in the amorphous hydrous zirconia. However, the more recent investigations of Zeng *et al.*[26] suggest that these interatomic distances are similar to those in m-ZrO_2. Stachs *et al.*[27] investigated the structural parameters of two zirconia xerogels. They found that local atomic ordering in the dried xerogel was similar to m-ZrO_2, whereas in the xerogel annealed at ≈300 °C it resembles t-ZrO_2.[27] The effect of lattice defects on the stabilization of a metastable t-ZrO_2 was investigated by Torralvo *et al.*[22] Osendi *et al.*[23] investigated the formation of metastable t-ZrO_2 by the thermal decomposition of the amorphous ZrO_2 precursor or zirconyl acetate, and they suggested that, initially, nucleation of t-ZrO_2 was favored by creation of anionic vacancies with trapped electrons. The electronic defects disappeared at high temperatures, the crystallites grew and nucleation of the m-ZrO_2 phase took place. Murase and Kato[24,25] examined the transformation of tetragonal ZrO_2 by ball-milling in different atmospheres. The obtained results indicated the important role of water adsorption on the surface of particles for the $t \rightarrow m$ transition of milled samples. The authors concluded that water vapor markedly accelerated crystallite growth of both m- and t-ZrO_2 and facilitated the transition, $t \rightarrow m$.

In this paper, we present a review of our investigations devoted to the stability of low temperature t-ZrO_2, which also include some new results (not published previously). In the light of these results, we discuss the proposed models of stabilization of low temperature t-ZrO_2.

CHARACTERIZATION OF ZIRCONIA PRODUCTS

The X-ray powder diffraction was a very important technique for the identification of ZrO_2 polymorphs. In our investigations, volume fractions of the *t*-ZrO_2 and *m*-ZrO_2 phases (v_t and v_m) were estimated from the integrated intensities of diffraction lines ($\bar{1}11$) and (111) of *m*-ZrO_2, and a diffraction line (101) of *t*-ZrO_2 following a procedure proposed by Toraya *et al.*[28] The volume fractions are given by the following equations:

$$v_m = \frac{1.311x}{1 + 0.311x} \quad , \tag{1}$$

where x is

$$x = \frac{I_m(\bar{1}11) + I_m(111)}{I_m(\bar{1}11) + I_m(111) + I_t(101)} \quad . \tag{2}$$

$$\nu_t = 1 - \nu_m \quad . \tag{3}$$

The crystallite size was estimated from the broadening of the diffraction lines (111) of *m*-ZrO_2, and (101) of *t*-ZrO_2 using the Scherrer equation:

$$D_{hkl} = \frac{0.9\lambda}{\beta_{hkl}\cos\theta} \quad , \tag{4}$$

λ being the X-ray wavelength (Cu-Kα), θ the Bragg angle, β_{hkl} the pure full width of the diffraction line (hkl) at half the maximum intensity.

The lattice strain (η_{hkl}) of the metastable *t*-ZrO_2 was estimated from the width of the diffraction lines 101 and 202 using the equation:

$$\beta_{hkl}\cos\theta = (0.9\lambda)/D^{o}_{hkl} + \eta_{hkl}\sin\theta \tag{5}$$

where D^{o}_{hkl} denotes the effective crystallite size. The values of β_{hkl} were found from the observed full width at half the maximum intensity (FWHM) of the diffraction lines, after correction for instrumental broadening, for which the corresponding width of the diffraction lines of α-SiO_2 was used, following the procedure given in literature.[29] Integrated intensities and FWHM of the diffraction lines were determined using the individual profile-fitting method (computer program PRO-FIT).[30]

Precise determinations of unit-cell parameters were performed using the powder-pattern fitting methods and α-Al_2O_3 (ZrO_2–Fe_2O_3 system) or α-Si (ZrO_2–Al_2O_3 system) as an internal standard. The Bragg angle positions, 2θ, of the diffraction lines were determined by the individual profile fitting method and taken as input data for the UNITCELL program.[31] Unit-cell pa-

rameters were then refined by the whole-powder-pattern decomposition method (WPPF program[28]). The fitting was performed in the scanned 2θ range, from 20° to 110°, using the split-type pseudo-Voigt profile function and the polynomial background model.

In some cases, the Fourier transform infrared (FT-IR) and laser Raman spectroscopy were also used as techniques complementary to XRD. Raman spectroscopy was often used for identification of ZrO_2 crystal phases.[32–46] This technique can sometimes be more convenient in distinguishing between the tetragonal and cubic ZrO_2 phases in relation to XRD.[44–46] In the case of laser Raman spectroscopy, volume fractions were determined from the intensities of the Raman-active modes of t-ZrO_2 at 267 and 148 cm^{-1}, as well as the Raman-active modes of m-ZrO_2 at 189 and 178 cm^{-1} following the procedure proposed by Clarke and Adar.[35] The volume fractions of m-ZrO_2 were estimated from the following equation:

$$v_m = \frac{I_m^{178} + I_m^{189}}{F(I_t^{148} + I_t^{267}) + I_m^{178} I_m^{189}} \quad , \tag{6}$$

where I_m and I_t correspond, respectively, to the intensities of the m-ZrO_2 and t-ZrO_2 Raman-active modes at the wave numbers, given as superscripts, while F is a factor close to unity (0.97).

Infrared spectroscopy was much less used, because only m-ZrO_2 could be easily recognized.[46–50] It can be seen from the group theory that t-ZrO_2 allows six Raman active modes of vibration ($A_{1g} + 2B_{1g} + 3E_g$) and only three IR active ($A_{2u} + 2E_u$). From these three allowed vibrations only one broad band with a transmittance minimum at ≈500 cm^{-1} was observed in the mid infrared region,[45–47] which could not be distinctly distinguished from the bands of cubic or amorphous zirconia. However, discoverry of two new IR active bands in the far infrared region, one at 177 cm^{-1}, typical of m-ZrO_2,[48] and the other, very strong and broad, with a transmittance minimum at ≈180 cm^{-1}, typical of t-ZrO_2,[48–50] enabled a distinct identification of the t-ZrO_2 phase.

SYNTHESIS OF METASTABLE t-ZrO_2

Metastable t-ZrO_2 can be obtained at RT and standard pressure by the thermal treatment of starting materials (zirconium salts, zirconium alkoxides or hydrous zirconia), as a product of solid state reactions,[51] by ball-milling m-ZrO_2,[13] and probably by ball-milling hydrous zirconia.[50] Most of the models presented were based on an examination of t-ZrO_2 products obtained by the wet chemical route,[3–9,15–27] which includes dissolving of zirconium

salts or alkoxides, formation of hydrous zirconia gel and crystallization of ZrO_2 by solid state calcination or hydrothermal treatment of hydrous zirconia gel. The synthesis conditions used to produce hydrous zirconia precursors strongly influence the phase composition of the ZrO_2 crystallization products.

Calcination of Hydrous Zirconia

The formation and the fraction of metastable *t*-ZrO_2 in the products of solid-state calcination of hydrous zirconia strongly depend on the processing parameters used during the preparation of hydrous zirconia precursors. Davis[52] found that precipitation of hydrous zirconia at high or low pH favors the formation of metastable *t*-ZrO_2 after calcination and cooling at temperatures between 400 and 600 °C, whereas the same thermal treatment of hydrous zirconia precipitated in neutral medium yielded *m*-ZrO_2. Srinivasan *et al.*[53,54] showed that, beside the pH of precipitation, the phase compositions of the ZrO_2 products depend on the time of precipitation[53] and the type of zirconium salt from which hydrous zirconia is produced.[54] Clearfield[55] discussed these observations and proposed the mechanism of hydrous zirconia precipitation.

In the succeeding investigation we examined the influence of mechanical treatment on the thermal behavior of hydrous zirconia.[50] Amorphous hydrous zirconia, precipitated from the aqueous solution of $ZrO(NO_3)_2 \cdot 2H_2O$ salt at pH = 10.5, was ball-milled at RT for up to 60 hours and the thermal behavior of the obtained samples was followed by differential scanning calorimetry (DSC) and thermogravimetric analysis (TGA). DSC curves of the samples contained an endothermic peak resulting from the dehydration and an exothermic peak resulting from the crystallization of samples (Figure 1). Samples obtained by ball-milling for 1, 3 and 9 hours showed two exothermic peaks due to crystallization of *t*-ZrO_2 as determined by XRD and FT-IR spectroscopy.[50] The presence of two exothermic peaks resulted from the heterogeneity of samples caused by ball-milling. TGA measurements showed continuous loss of weight in a temperature range between 50 °C and 400 °C. Further heating up to ≈850 °C caused a very small weight loss. The results of DSC and TGA indicate that ball-milling of hydrous zirconia causes dehydration, an increase in crystallization temperature and a decrease in the enthalpy of ZrO_2 crystallization. Dehydration has no influence on the increase in crystallization temperature and the decrease in the heat flow of crystallization. No change of weight in the temperature region corresponding to the exothermic peaks of crystallization indicates that crystallization of a metastable *t*-ZrO_2 from hydrous zirconia is not a simple topotactic process.

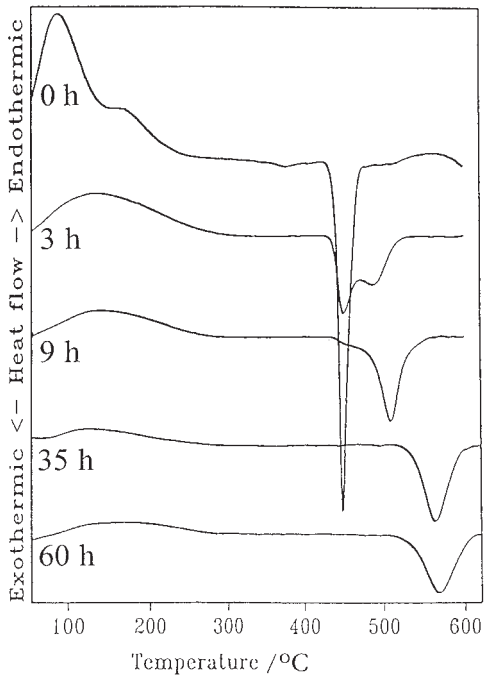

Figure 1. DSC curves of the hydrous zirconia samples precipitated at pH = 10.5 from aqueous solution of $ZrO(NO_3)_2 \cdot 2H_2O$ salt and mechanically treated for up to 60 h.

The above presented investigation was continued.[56,57] Hydrous zirconia samples, obtained by rapid precipitation at pH = 2.5, 7.5 and 10.5, were subjected to the influence of mechanical treatment (ball-milled up to 60 hours) [56] or γ-irradiation (dose rates of 5.6 Gy s^{-1} up to a final dose of 20 MGy).[57]

Figure 2 illustrates the dependence of the crystallization temperature of hydrous zirconia, precipitated at three different pH values, on the time of ball-milling. The obtained curves indicate that, in all cases, an early stage of ball-milling leads to an increase in the crystallization temperature, and also that the extent of this effect depends on the precipitation pH. In the first hour of ball-milling, the crystallization temperature increased by ≈5 °C for the sample precipitated at pH = 10.5, ≈15 °C for the sample precipitated at pH = 7.5 and ≈50 °C for the sample precipitated at pH = 2.5, thus suggesting that a higher pH of the precipitation produced tougher grains of hydrous zirconia, more resistant to the disordering process caused by ball-milling. With prolonged ball-milling, the maximum values of crystallization temperature were reached, and then the crystallization temperature decreased with further ball-milling. The time of ball-milling needed to obtain the maximum crystallization temperature increased with the increase in the precipi-

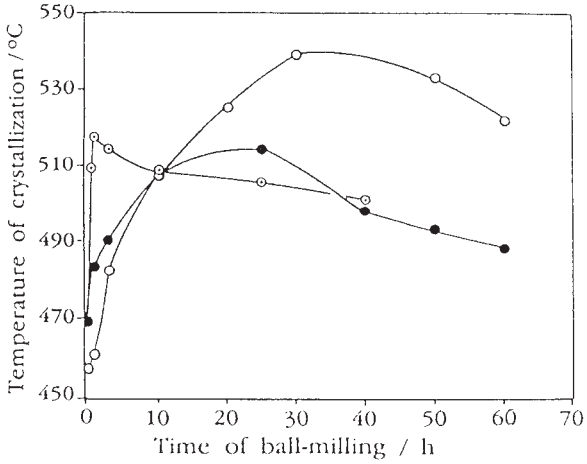

Figure 2. The temperature of crystallization of hydrous zirconia as a function of ball-milling time. Symbols ○, ● and ⊙ stand for precipitation pH values of 10.5, 7.5 and 2.5, respectively.

tation pH of hydrous zirconia from 1 hour at pH = 2.5, 20 hours at pH = 7.5 to 35 hours at pH = 10.5. It is interesting to note that at the point corresponding to 10 hours of ball-milling the crystallization temperature was independent of the pH of the precipitation.

The results of phase analysis, obtained after calcination and cooling from 600 °C to RT inside a DSC instrument, are given in Table II. Phase compositions of the crystallization products of starting samples (not subjected to mechanical treatment) were pH dependent in a way similar to that described by Davis.[52] However, phase compositions of the samples subjected to mechanical treatment showed that regardless of the precipitation pH, the first stage of ball-milling (related to the increase in crystallization temperature) resulted in the formation of pure t-ZrO_2. The second stage of ball-milling (related to the decrease in crystallization temperature) resulted in the formation of m-ZrO_2. The influence of mechanical treatment on the thermal behavior of hydrous zirconia is illustrated by the following scheme:

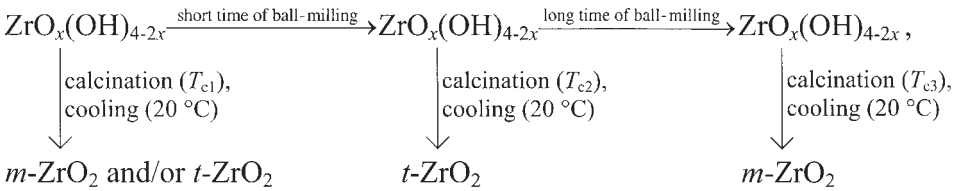

TABLE II

The results of DSC analysis (enthalpy and temperature of crystallization) of ball-milled hydrous zirconia precipitated at pH = 2, 7 and 10.5 and the results of phase analysis (laser Raman spectroscopy) of the corresponding crystallization products

pH	Time of ball-milling/ h	ΔH_c / kJ mol^{-1}	T_{c1} / °C	T_{c2} / °C	Phase composition (volume fractions)
2.5	0	–13	469	–	t-ZrO_2 (0.67) + m-ZrO_2 (0.33)
	1	–14	515	–	t-ZrO_2
	3	–16	514	–	t-ZrO_2 (0.99) + m-ZrO_2 (0.01)
	10	–19	508	–	–
	25	–14	506	–	m-ZrO_2 (0.52) + t-ZrO_2 (0.48)
	40	–13	501	–	m-ZrO_2 (0.80) + t-ZrO_2 (0.20)
7.5	0	–20	468	–	m-ZrO_2
	1	–20	473	503	t-ZrO_2
	3	–20	473	507	–
	10	–20	507	–	–
	25	–20	514	–	t-ZrO_2
	40	–20	498	–	m-ZrO_2 + t-ZrO_2
	50	–19	493	–	m-ZrO_2 (0.70) + t-ZrO_2 (0.30)
	60	–19	488	–	–
10.5	0	–21	457	–	t-ZrO_2
	1	–20	460	478	–
	3	–19	465	489	t-ZrO_2
	10	–18	507	–	t-ZrO_2
	20	–14	525	–	t-ZrO_2
	30	–12	539	–	–
	50	–11	533	–	m-ZrO_2 (0.52) + t-ZrO_2 (0.48)
	60	–11	522	–	m-ZrO_2 + t-ZrO_2

where T_{c1}, T_{c2} and T_{c3} stand for temperatures of crystallization mutually related $T_{c1} < T_{c3} < T_{c2}$.

Unlike the mechanical treatment, γ-irradiation had no influence on the thermal behavior of hydrous zirconia. However, the results of microelectrophoretic measurements showed that γ-irradiation influenced the surface properties of hydrous zirconia in dependence on the precipitation pH.[57] Hy-

drous zirconia, precipitated at pH = 2, proved to be the most susceptible to γ-irradiation, while the same γ-irradiation had very little (if any) influence on the surface properties of hydrous zirconia precipitated at pH = 10.5. After γ-irradiation, the electrophoretic mobility of hydrous zirconia, precipitated at pH = 2, increased at both low and high pH, thus indicating an increase in its adsorption capacity (Figure 3). The obtained results suggest that the susceptibility of hydrous zirconia to the influence of ball-milling and γ-irradiation increases with a decrease in precipitation pH.

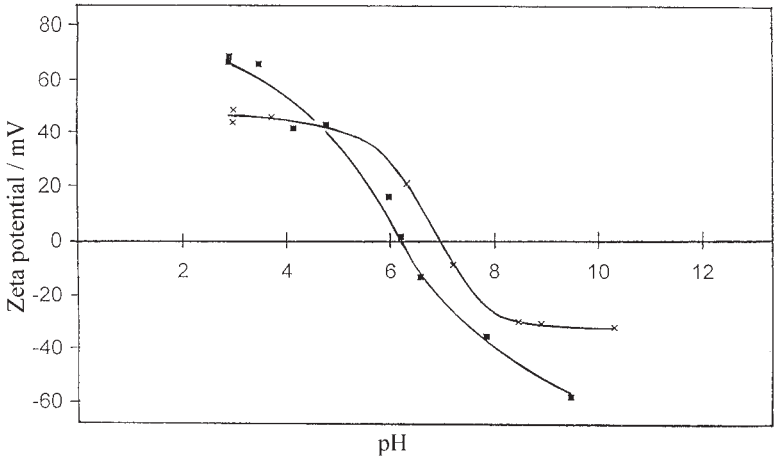

Figure 3. Zeta potential, measured for hydrous zirconia samples precipitated at pH = 2. Symbols ■ and × stand for γ-irradiated and nonirradiated samples, respectively.

Hydrothermal Crystallization of Zirconia

In general, the hydrothermal treatment of hydrous zirconia yields well-shaped and isolated fine ZrO_2 particles, while the solid-state calcination strongly affects the morphology and particle size due to the sintering effect. The hydrothermal method is, therefore, preferred in the production of fine zirconia powders for use in advanced ceramics. Hydrothermal treatment of highly acidic solutions or suspensions of hydrous zirconia produced monoclinic zirconia, *m*-ZrO_2,[58–60] whereas hydrothermal treatment at high pH values yielded, besides *m*-ZrO_2, a metastable *t*-ZrO_2 and also a metastable cubic zirconia, *c*-ZrO_2, in the presence of $CaCl_2$[61] or NaOH[62,63] as a stabilizing agent. The mechanism of hydrothermal crystallization of zirconia was investigated in several papers.[9,21,64] Tani *et al.*[19] concluded that the formation of *m*-ZrO_2 by the hydrothermal treatment proceeded *via* a dissolution/precipitation mechanism,[19,60] whereas the formation of *t*-ZrO_2 occurred as a result

of structural rearrangement of amorphous hydrous zirconia (topotactic crystallization).[19] Denkewicz *et al.*[21] proposed a model of hydrothermal crystallization of ZrO_2 based on three control regimes. At low pH the solubility is high, and the hydrothermal crystallization occurs *via* a dissolution/precipitation mechanism producing *m*-ZrO_2. In a neutral or mild acidic medium, solubility is very low, so that crystallization occurs *in situ* by structural (topotactic) rearrangement of hydrous zirconia. The product of hydrothermal crystallization in this region will be predominantly *t*-ZrO_2, and the presence of *m*-ZrO_2 can be attributed to the transformation *t*-$ZrO_2 \rightarrow$ *m*-ZrO_2 with a prolonged hydrothermal treatment. At high pH, the solubility of hydrous zirconia is very high and similar to the solubility at low pH; yet, *in situ* topotactic crystallization prevails because of a higher energy state of the obtained hydrous zirconia gel.[21]

Our previous investigation[50] has shown that the formation of a metastable *t*-ZrO_2 during the solid state calcination of hydrous zirconia is not a simple topotactic process. For this reason, in the following research we examined the mechanism of the hydrothermal crystallization of ZrO_2 at different pH.[63] Aqueous suspensions of hydrous zirconia at pH = 2, 7, 9.5 and 13, prepared by the addition of NaOH to the solution of $ZrO(NO_3)_2 \cdot 2H_2O$ salt, were hydrothermally treated at 95 °C for different times. Phase compositions of the obtained products, determined using XRD and laser Raman spectroscopy, are given in Table III. The kinetics of zirconia crystallization during hydrothermal treatments was determined from the decrease in the exothermic peak of crystallization in the corresponding DSC curves. Hydrothermal crystallization was found to proceed much more slowly in a neutral pH medium than in an acidic or alkaline medium (Figure 4).

Although our crystallization kinetic observations can be accommodated within the model of Denkewicz *et al.*,[21] our phase analysis results differ from the results expected on the basis of this model. The model of Denkewicz *et al.*[21] is based on the conclusion that the dissolution/precipitation mechanism can produce only *m*-ZrO_2, while a metastable *t*-ZrO_2 appears exclusively during *in situ* topotactic crystallization of hydrous zirconia. On the other hand, if hydrothermal crystallization proceeds *via* the dissolution/precipitation mechanism in the whole pH range, it can be concluded that both *m*-ZrO_2 and *t*-ZrO_2 could be produced by this mechanism. Our X-ray powder diffraction results, as well as the results of Morgan[59] and Kato *et al.*,[65] showed that even at low pH, *m*-ZrO_2 is not the exclusive product formed by the dissolution/precipitation mechanism during hydrothermal crystallization. Hydrous zirconia precipitated at pH = 2 crystallized first to some metastable form of zirconium nitrate, which under prolonged hydrothermal treatment transformed into *m*-ZrO_2. Also, the results of phase analysis of sam-

TABLE III

The results of DSC analysis (enthalpy, temperature and percentage of crystallization) and phase analysis (XRD and laser Raman spectroscopy) of the hydrothermally treated hydrous zirconia samples precipitated at different pH

pH	Hydrotherm. treatment	DSC			Phase composition (volume fractions)
		Enthalpy	Peak max.	Crystall.	
	h	kJ mol^{-1}	°C	%	
2	0	–12	451	0	amorphous
	8	–7	458	42	»zirconium nitrate« + $NaNO_3$
	60	0	–	100	–
	100	0	–	100	»zirconium nitrate« + $NaNO_3$
	300	–	–	–	m-ZrO_2
7	0	–19	457	0	amorphous
	220	–17	458	9	amorphous
	300	–14	469	27	–
	500	–9	501	51	–
	750	–5	464	75	m-ZrO_2 (0.75) + t-ZrO_2 + c-ZrO_2
	1400	0	–	100	m-ZrO_2 (0.77) + t-ZrO_2 + c-ZrO_2
9.5	0	–21	461	0	amorphous
	25	–16	485	25	–
	75	–8	529	63	amorphous
	170	–1	572	95	c-ZrO_2 + amorphous
	700	0	–	100	c-ZrO_2 + amorphous
13	0	–19	475	0	amorphous
	1	–13	526	32	–
	3	–6	540	65	amorphous
	7	0	–	100	m-ZrO_2 (0.68) + c-ZrO_2
	24	0	–	100	m-ZrO_2 (0.70) + c-ZrO_2

ples precipitated at pH = 7 and 13 indicated that the presence of m-ZrO_2 cannot be attributed to the t-$ZrO_2 \rightarrow m$-ZrO_2 transformation caused by hydrothermal treatment, as suggested by Denkewicz *et al.*[21] The obtained results show that both m-ZrO_2 and metastable t- or c-ZrO_2 phases appear as products of hydrothermal crystallization of hydrous zirconia precipitated at pH = 7 and 13. The phase fractions remain approximately the same after a prolonged hydrothermal treatment, indicating that the presence of m-ZrO_2

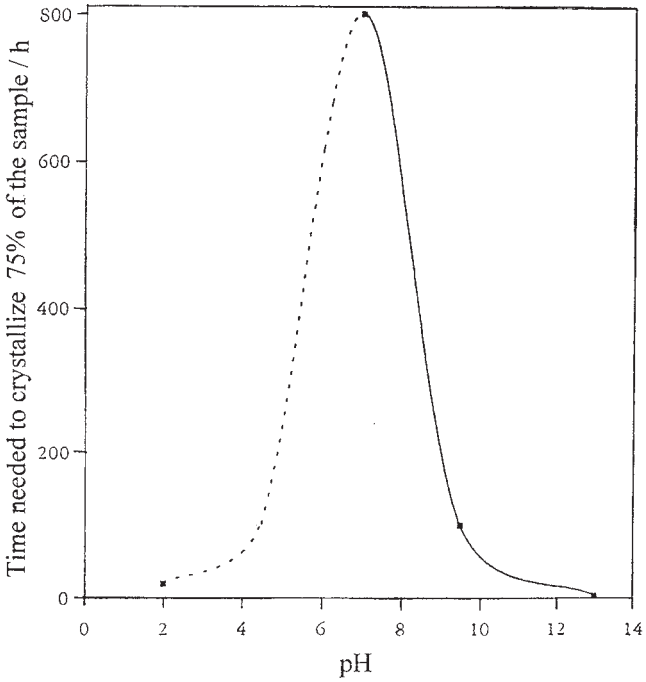

Figure 4. The time needed to crystallize 75% of the sample as a function of pH.

cannot be attributed to the t-$ZrO_2 \rightarrow m$-ZrO_2 transformation. No evidence of the existence of a gel structure controlled regime[21] could be found by the phase analysis of the products of hydrothermal treatment. It can be concluded that *in situ* crystallization of amorphous hydrous zirconia, if it occurs, is not a topotactic process.

The analogy between the rate of the hydrothermal crystallization of ZrO_2 and solubility of hydrous zirconia[66] indicates that hydrothermal crystallization proceeds *via* the dissolution/precipitation mechanism in the whole pH range.

Thermal Decompositions of Zirconium Salts

Zirconium salts have well-defined structures, compared to hydrous zirconia, which enable an easier insight into the mechanism of t-ZrO_2 formation by thermal decomposition of these salts. However, formation of ZrO_2 by thermal decomposition of zirconium salts was surprisingly little investigated compared to wet chemical procedures. For this reason, we investigated

the phase development of the thermal decomposition products of three different zirconium salts ($ZrOCl_2 \cdot 8H_2O$, $ZrO(NO_3)_2 \cdot 2H_2O$ and $Zr(SO_4)_2 \cdot 4H_2O$) calcinated at selected temperatures up to 1300°C.[48] Chemical and structural changes in the solids were monitored after cooling to RT by X-ray powder diffraction, FT-IR and laser Raman spectroscopy. The results of phase analysis are given in Table IV. The obtained results show that the transformation from the starting salt to ZrO_2 proceeds through an amorphous intermediary. In all three cases, the first crystallization product contained, besides *m*-ZrO_2, a metastable *t*-ZrO_2. However, the volume fraction of the metastable phase depended on the nature of the starting salt. The first crys-

TABLE IV

The results of phase analysis of the thermal decomposition products of zirconium salts, obtained after calcination at the atmospheric pressure of air and cooling to room temperature

Salt	Temp. °C	Phase composition (volume fractions)	Remark[a]
$ZrOCl_2 \cdot 8H_2O$	–	$ZrOCl_2 \cdot 8H_2O$	SDL
	300	amorphous	
	400	*t*-ZrO_2 (0.97) + *m*-ZrO2 (0.03)	BDL
	700	*m*-ZrO_2 (0.96) + *t*-ZrO_2 (0.04)	LBDL
	1300	*m*-ZrO_2	SDL
$ZrO(NO_3)_2 \cdot 2H_2O$	–	$ZrO(NO_3)_2 \cdot 2H_2O$	SDL
	300	amorphous	
	400	*m*-ZrO_2 (0.51) + *t*-ZrO_2 (0.49)	VBDL
	700	*m*-ZrO_2 (0.62) + *t*-ZrO_2 (0.38)	VBDL
	1300	*m*-ZrO_2 (0.95) + *t*-ZrO_2 (0.05)	BDL
	300	*m*-ZrO_2	SDL
$Zr(SO_4)_2 \cdot 4H_2O$	–	$Zr(SO_4)_2 \cdot 4H_2O$	gradual decrease of peak intensities and increase of diffraction lines broadening
	200	$Zr(SO_4)_2 \cdot 4H_2O$	
	300	$Zr(SO_4)_2 \cdot 4H_2O$	
	600	amorphous	
	700	*m*-ZrO_2 (0.77) + *t*-ZrO_2 (0.23)	BDL
	1300	*m*-ZrO_2 (0.97) + *t*-ZrO_2 (0.03)	LBDL

[a]Descriptions: SDL = sharp diffraction lines, LBDL = little broadened diffraction lines, BDL = broadened diffraction lines, VBDL = very broadened diffraction lines.

tallization products of $ZrO(NO_3)_2 \cdot 2H_2O$ and $Zr(SO_4)_2 \cdot 4H_2O$ salts contained m-ZrO_2 as the dominant phase, whereas the corresponding product of $ZrOCl_2 \cdot 8H_2O$ contained a metastable t-ZrO_2 as the dominant phase with

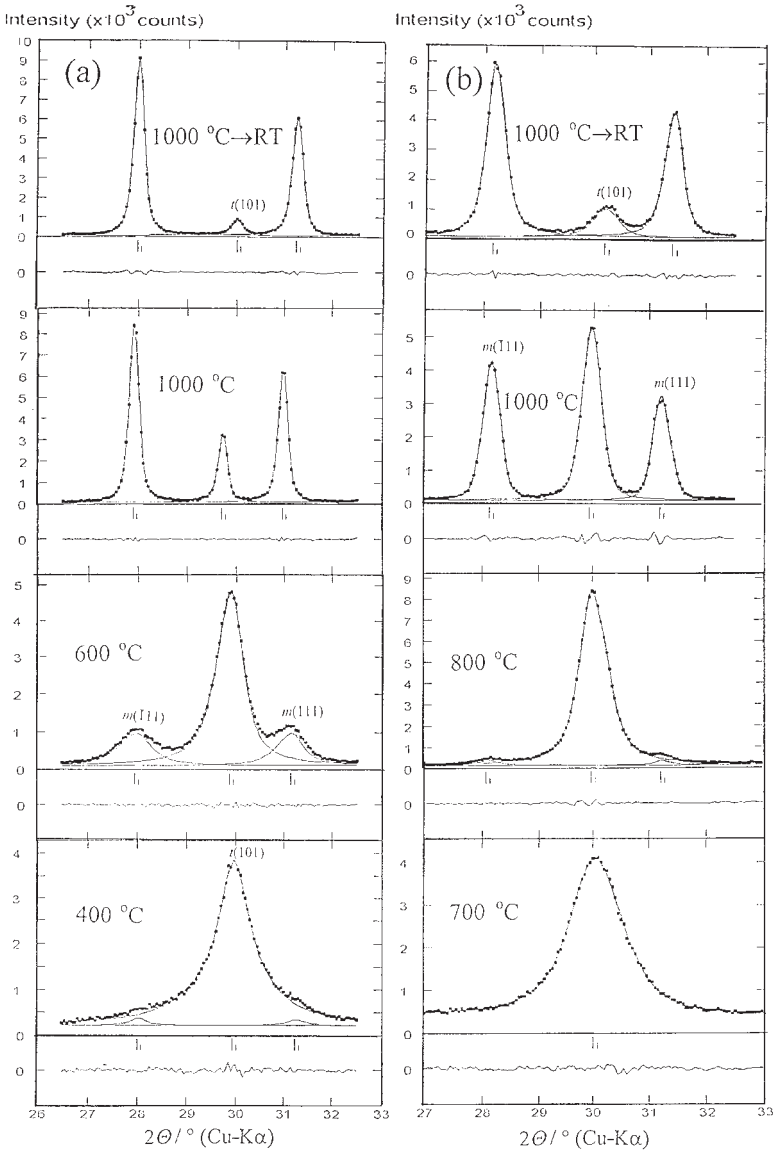

Figure 5. Individual profile fitting results obtained during the heating of the thermal decomposition product of $ZrO(NO_3)_2 \cdot 2H_2O$ salt (a) and $Zr(SO_4)_2 \cdot 4H_2O$ salt (b) in the presence of air at atmospheric pressure ($\approx 10^5$ Pa).

TABLE V

Results of the *in situ* phase analysis during the heating of the thermal decomposition products of zirconium salts in the presence of air at atmospheric pressure ($\approx 10^5$ Pa) and low pressure ($\approx 2 \times 10^{-3}$ Pa)[69]

Sample	Treatment	Phase composition (volume fractions)	
		Atmospheric pressure	Low pressure
ZN	350 °C	amorphous	amorphous
	400 °C	t-ZrO_2 (0.96) + m-ZrO_2 (0.04)	–
	500 °C	t-ZrO_2 (0.80) + m-ZrO_2 (0.20)	–
	600 °C	t-ZrO_2 (0.65) + m-ZrO_2 (0.35)	t-ZrO_2
	800 °C	m-ZrO_2 (0.72) + t-ZrO_2 (0.28)	–
	900 °C	m-ZrO_2 (0.79) + t-ZrO_2 (0.21)	–
	1000 °C	m-ZrO_2 (0.87) + t-ZrO_2 (0.13)	–
	1200 °C	–	t-ZrO_2
	– cooling to RT	m-ZrO_2 (0.96) + t-ZrO_2 (0.04)	t-ZrO_2 (0.88) + m-ZrO_2 (0.12)
	– exposure to air at RT	–	m-ZrO_2 (0.54) + t-ZrO_2 (0.46)
ZS1	–	amorphous	–
	700 °C	t-ZrO_2	–
	800 °C	t-ZrO_2 (0.95) + m-ZrO_2 (0.05)	–
	900 °C	t-ZrO_2 (0.71) + m-ZrO_2 (0.29)	–
	1000 °C	m-ZrO_2 (0.61) + t-ZrO_2 (0.39)	–
	– cooling to RT	m-ZrO_2 (0.92) + t-ZrO_2 (0.08)	–
ZS2	–	–	am + ZS + t-ZrO_2 + m-ZrO_2
	600 °C	–	t-ZrO_2(0.69) + m-ZrO_2(0.31) + ZS
	700 °C	–	t-ZrO_2(0.82) + m-ZrO_2(0.18) + ZS
	800 °C	–	t-ZrO_2(0.89) + m-ZrO_2(0.11) + ZS
	900 °C	–	t-ZrO_2(0.92) + m-ZrO_2(0.08) + ZS
	1000 °C	–	t-ZrO_2 (0.90) + m-ZrO_2 (0.10)
	1200 °C	–	t-ZrO_2 (0.80) + m-ZrO_2 (0.20)
	– cooling to RT	–	t-ZrO_2 (0.69) + m-ZrO_2 (0.31)
	– exposure to air at RT	–	m-ZrO_2 (0.55) + t-ZrO_2 (0.45)

[a]Description: ZN = $ZrO(NO_3)_2 \cdot 2H_2O$ salt (Ventron) calcinatied at 330 °C in air for 2 h, and then cooled to RT; ZS1 = $Zr(SO_4)_2 \cdot 4H_2O$ salt (The British Drug Houses Ltd.) calcinated at 600 °C in air for 2 h, and then cooled to RT; ZS2 = $Zr(SO_4)_2 \cdot 4H_2O$ salt (Hopkins & Williams Ltd.) calcinated at 650 °C in air for 2 h, and then cooled to RT; ZS = zirconium sulfate; am = amorphous.

only traces of m-ZrO_2. Further increase in temperature treatment caused a decrease in the t-ZrO_2 content, but the rate of this process varied for different salts (highest for $ZrOCl_2 \cdot 8H_2O$ and lowest for $Zr(SO_4)_2 \cdot 4H_2O$). These

results show that the metastable t-ZrO_2 content in thermal decomposition products is not related to its susceptibility.

Similarity between the structural parameters (Zr–Zr and Zr–O distances) of the $ZrOCl_2 \cdot 8H_2O$ salt and of t-ZrO_2[20,67] supports the model of Livage *et al.*[17] However, since the phase compositions were determined at RT, the observed differences could result from the t-$ZrO_2 \rightarrow m$-ZrO_2 transformation on cooling. The presence of this kind of transformation was observed by the *in situ* phase analysis of the crystallization products of hydrous zirconia.[68–70] It was found[69,70] that, regardless of the precipitation pH, hydrous zirconia crystallized as a metastable t-ZrO_2, which may or may not transform into m-ZrO_2 during cooling to RT.

In order to examine the influence of cooling, we undertook an *in situ* X-ray powder diffraction study of the thermal decomposition products of $ZrO(NO_3)_2 \cdot 2H_2O$ and $Zr(SO_4)_2 \cdot 4H_2O$ salts. The results of phase analysis obtained during calcination in the presence of air at atmospheric pressure ($\approx 10^5$ Pa)[71] and low pressure ($\approx 2 \times 10^{-3}$ Pa)[72] are given in Table V.

In both cases, calcination caused crystallization of the amorphous precursors into t-ZrO_2, which, during the cooling or further calcination in the presence of air at atmospheric pressure, transformed into m-ZrO_2 (Figure 5). On the other hand, during the calcination in vacuum ($\approx 2 \times 10^{-3}$ Pa), this metastable phase remained stable up to 1200°C.[72] The thermodynamically stable m-ZrO_2 appeared after cooling of samples to RT. If cooling was performed at low air pressure, the m-ZrO_2 content was small. The introduction of air, even at RT, caused a considerable increase in m-ZrO_2, which in all cases became the dominant phase (Table V). The obtained results indicate that, regardless of the structural difference, the products of thermal decomposition of zirconium salts crystallize into a metastable t-ZrO_2, which, during cooling or further calcination, transforms into m-ZrO_2. An important role of oxygen in the t-$ZrO_2 \rightarrow m$-ZrO_2 transformation indicates that the lack of oxygen in the zirconia lattice favors the formation of a metastable t-ZrO_2. The effects of calcination in the presence of air at atmospheric pressure or in vacuum are summarized in the following scheme:

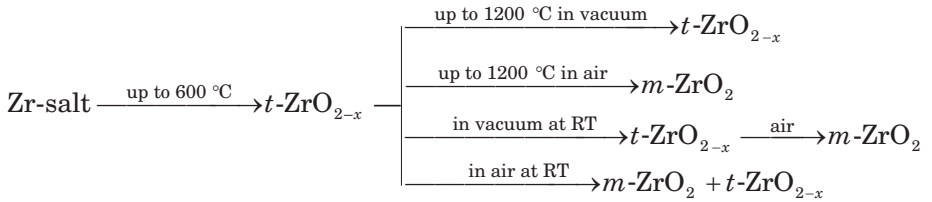

STABILITY OF LOW TEMPERATURE t-ZrO_2

The transformation from t-ZrO_2 to m-ZrO_2 exhibits many of the characteristics typical of the martensitic transformation in metals. This transformation causes volume expansion from 3 to 5%, used in the transformation toughening of ceramic material.[1,73] Crack propagation generates stress in ceramic material, which can cause transformation of the small metastable t-ZrO_2 particles incorporated in the bulk of the ceramic material. Volume expansion of the transformed particles generates compressive strain in the vicinity of the crack, so extra work would be required to move the crack through the ceramic material.[1] During tailoring of the ceramics with improved toughness, it is important to know the stability of the t-ZrO_2 particles. If their stability is very small, the phase transformation will occur spontaneously. On the other hand, if their stability is high, t-ZrO_2 particles will not transform. This fact can be exploited to toughen zirconia ceramics, as well as other ceramics, *e.g*. alumina containing zirconia.

In the succeeding research, we examined the influence of processing parameters (pH value, type of ions, and reaction temperature) on the properties of hydrous zirconia, precipitated from aqueous solution of zirconium salts[74–76] or prepared by hydrolytic polycondensation of zirconium n-propoxide,[77,78] and the stability of the corresponding t-ZrO_2 crystallization products. In order to determine the stability of t-ZrO_2, the obtained crystallization products were subjected to the influence of temperature (2 hours at 600 or 800 °C), pressure (2 minutes at 500, 1000 or 1350 MPa using a Carver press) and γ-irradiation (with a dose rate of 5.6 Gy s^{-1} up to a final dose of 10 MGy using a ^{60}Co source at the Ruđer Bošković Institute). All the samples were shown to be stable under high γ-irradiation.[75,76] On the other hand, the sensitivity of the metastable t-ZrO_2 to the influence of temperature and pressure strongly depended on the preparation conditions.

The notation of the hydrous zirconia samples, synthesized by hydrolytic polycondensation of zirconium n-propoxide (Aldrich), and the corresponding synthesis conditions are given in Table VI.

Most of the crystallization products, obtained on calcination of samples at 400 °C, contained t-ZrO_2 as the dominant phase (Table VII). The stability of t-ZrO_2 to the influence of pressure (1350 MPa) decreased with an increase in the processing pH up to 7.5 (Figure 6). Further increase in pH value caused an increase in the stability of t-ZrO_2. Reaction temperature also influenced the stability of the obtained t-ZrO_2 products. Metastable t-ZrO_2 products of the samples subjected to the hydrolytic polycondensation reaction at 100 °C proved to be much more susceptible to the influence of pressure than the metastable t-ZrO_2 products of the samples obtained from the same reaction mixture at RT.[78]

TABLE VI

Experimental conditions for the preparation of hydrous zirconia samples

Sample	Chemical composition of the reactants	pH	Treatment
Z1	15 ml 70% (*w*) $Zr(OCH_2CH_2CH_3)_4$, 15 ml 1-C_3H_7OH, 23 ml H_2O, 2 ml 65% HNO_3(aq)	<1	Refluxing for 2 h at 100 °C, washing with H_2O and drying at 70 °C for 24 h
Z2	15 ml 70% (*w*) $Zr(OCH_2CH_2CH_3)_4$, 15 ml 1-C_3H_7OH, 23 ml H_2O, 2 ml 38% HCl(aq)	1	Refluxing for 2 h at 100 °C, washing with H_2O and drying at 70 °C for 24 h
Z3	15 ml 70% (*w*) $Zr(OCH_2CH_2CH_3)_4$, 35 ml 1-C_3H_7OH, 49 ml H_2O, 1 ml 65% HNO_3(aq)	1.5	Refluxing for 2 h at 100 °C, washing with H_2O and drying at 70 °C for 24 h
Z4	15 ml 70% (*w*) $Zr(OCH_2CH_2CH_3)_4$, 35 ml 1-C_3H_7OH, 49.5 ml H_2O, 0.5 ml 65% HNO_3(aq)	3	Refluxing for 2 h at 100 °C, washing with H_2O and drying at 70 °C for 24 h
Z5	15 ml 70% (*w*) $Zr(OCH_2CH_2CH_3)_4$, 35 ml 1-C_3H_7OH, 50 ml H_2O	6	Refluxing for 2 h at 100 °C, washing with H_2O and drying at 70 °C for 24 h
Z6	15 ml 70% (*w*) $Zr(OCH_2CH_2CH_3)_4$, 35 ml 1-C_3H_7OH, 50 ml H_2O	6	Washing with H_2O and drying at 70°C for 24 h
Z7	15 ml 70% (*w*) $Zr(OCH_2CH_2CH_3)_4$, 35 ml 1-C_3H_7OH, 50 ml 0.5 M NH_4NO_3(aq)	7.5	Refluxing for 2 h at 100 °C, washing with H_2O and drying at 70 °C for 24 h
Z8	15 ml 70% (*w*) $Zr(OCH_2CH_2CH_3)_4$, 35 ml 1-C_3H_7OH, 30 ml H_2O, 20 ml 25% NH_3(aq)	10.5	Refluxing for 2 h at 100 °C, washing with H_2O and drying at 70 °C for 24 h
Z9	15 ml 70% (*w*) $Zr(OCH_2CH_2CH_3)_4$, 35 ml 1-C_3H_7OH, 30 ml H_2O, 20 ml 25% NH_3(aq)	10.5	Washing with H_2O and drying at 70 °C for 24 h
Z10	15 ml 70% (*w*) $Zr(OCH_2CH_2CH_3)_4$, 35 ml 1-C_3H_7OH, 47 ml H_2O, 3 ml 25% $(C_2H_5)_4NOH$(aq)	13	Refluxing for 2 h at 100 °C, washing with H_2O and drying at 70 °C for 24 h
Z11	15 ml 70% (*w*) $Zr(OCH_2CH_2CH_3)_4$, 35 ml 1-C_3H_7OH, 47 ml H_2O, 3 ml 25% $(C_2H_5)_4NOH$(aq)	13	Washing with H_2O and drying at 70 °C for 24 h
Z12	15 ml 70% (*w*) $Zr(OCH_2CH_2CH_3)_4$, 35 ml 1-C_3H_7OH, 38 ml H_2O, 12 ml 1.5 M NaOH(aq)	>13	Refluxing for 2 h at 100 °C, washing with H_2O and drying at 70 °C for 24 h

TABLE VII

Phase composition of the samples subjected to the influence of temperature and pressure

Sample	Treatment	Phase composition (volume fractions)	D_{hkl}/ nm	
			t-ZrO_2	m-ZrO_2
Z1	–	amorphous	–	–
	400 °C	t-ZrO_2	15.5	–
	400 °C + 800 °C	t-ZrO_2 (0.74) + m-ZrO_2 (0.26)	23.3	21.7
	400 °C + 800 °C[a]	t-ZrO_2 (0.76) + m-ZrO_2 (0.24)	31.1	23.1
	400 °C + 500 MPa	t-ZrO_2 (0.84) + m-ZrO_2 (0.16)	14.6	10.8
	400 °C + 1350 MPa	t-ZrO_2 (0.64) + m-ZrO_2 (0.36)	14.0	11.0
Z2	–	amorphous	–	–
	400 °C	t-ZrO_2 (0.86) + m-ZrO_2 (0.14)	14.4	17.2
	400 °C + 600 °C	t-ZrO_2 (0.51) + m-ZrO_2 (0.49)	20.5	16.9
	400 °C + 800 °C	m-ZrO_2 (0.93) + t-ZrO_2 (0.07)	–	18.9
	400 °C + 500 MPa	t-ZrO_2 (0.74) + m-ZrO_2 (0.26)	11.9	13.3
	400 °C + 1350 MPa	t-ZrO_2 (0.52) + m-ZrO_2 (0.48)	9.4	10.8
Z3	–	amorphous	–	–
	400 °C	t-ZrO_2 (0.98) + m-ZrO_2 (0.02)	14.7	–
	400 °C + 600 °C	t-ZrO_2 (0.85) + m-ZrO_2 (0.15)	18.7	–
	400 °C + 800 °C	t-ZrO_2 (0.55) + m-ZrO_2 (0.45)	20.5	17.1
	400 °C + 500 MPa	t-ZrO_2 (0.74) + m-ZrO_2 (0.26)	20.1	17.7
	400 °C + 1000 MPa	t-ZrO_2 (0.64) + m-ZrO_2 (0.36)	17.6	14.4
	400 °C + 1350 MPa	t-ZrO_2 (0.53) + m-ZrO_2 (0.47)	11.0	10.9
Z4	–	amorphous	–	–
	400 °C	t-ZrO_2 (0.81) + m-ZrO_2 (0.19)	18.7	6.7
	400 °C[a]	t-ZrO_2 (0.88) + m-ZrO_2 (0.12)	19.0	11.8
	400 °C + 600 °C	t-ZrO_2 (0.65) + m-ZrO_2 (0.35)	18.9	17.6
	400 °C + 600 °C[a]	t-ZrO_2 (0.70) + m-ZrO_2 (0.30)	20.8	19.3
	400 °C + 800 °C	m-ZrO_2 (0.90) + t-ZrO_2 (0.10)	20.3	20.7
	400 °C + 800 °C[a]	m-ZrO_2 (0.84) + t-ZrO_2 (0.16)	23.3	22.8
	400°C[a] + 500 MPa	t-ZrO_2 (0.56) + m-ZrO_2 (0.44)	20.1	18.1
	400°C[a] +1350 MPa	m-ZrO_2 (0.64) + t-ZrO_2 (0.36)	19.1	16.3
Z5	–	amorphous	–	–
	400 °C	t-ZrO_2 (0.62) + m-ZrO_2 (0.38)	8.6	9.1

continued

TABLE VII (cont.)

Sample	Treatment	Phase composition (volume fractions)	D_{hkl}/ nm	
			t-ZrO_2	m-ZrO_2
	400 °C + 600 °C	m-ZrO_2 (0.76) + t-ZrO_2 (0.24)	14.3	14.7
	400 °C + 600 °C[a]	m-ZrO_2 (0.66) + t-ZrO_2 (0.34)	15.5	15.6
	400 °C + 800 °C	m-ZrO_2 (0.94) + t-ZrO_2 (0.06)	16.4	19.8
	400 °C + 500 MPa	m-ZrO_2 (0.65) + t-ZrO_2 (0.35)	8.1	8.8
	400 °C + 1000 MPa	m-ZrO_2 (0.85) + t-ZrO_2 (0.15)	7.8	8.5
	400 °C + 1350 MPa	m-ZrO_2 (0.90) + t-ZrO_2 (0.10)	5.9	8.0
Z6	–	amorphous	–	–
	400 °C	t-ZrO_2 (0.79) + m-ZrO_2 (0.21)	16.3	10.3
	400 °C + 600 °C	m-ZrO_2 (0.59) + t-ZrO_2 (0.41)	15.6	14.2
	400 °C + 800 °C	m-ZrO_2 (0.94) + t-ZrO_2 (0.06)	13.9	17.8
	400 °C + 500 MPa	t-ZrO_2 (0.54) + m-ZrO_2 (0.46)	–	–
	400 °C + 1000 MPa	m-ZrO_2 (0.59) + t-ZrO_2 (0.41)	16.7	10.4
Z7	–	amorphous	–	–
	400 °C	t-ZrO_2 (0.69) + m-ZrO_2 (0.31)	10.0	8.9
	400 °C + 600 °C	m-ZrO_2 (0.84) + t-ZrO_2 (0.16)	15.0	14.0
	400 °C + 800 °C	m-ZrO_2 (0.95) + t-ZrO_2 (0.05)	26.7	23.1
	400 °C + 500 MPa	m-ZrO_2 (0.75) + t-ZrO_2 (0.25)	7.4	8.8
	400 °C + 1350 MPa	m-ZrO_2 (0.94) + t-ZrO_2 (0.06)	6.8	8.0
Z8	–	amorphous	–	–
	400 °C	t-ZrO_2 (0.88) + m-ZrO_2 (0.12)	9.7	9.8
	400 °C + 600 °C	t-ZrO_2 (0.64) + m-ZrO_2 (0.36)	12.2	12.1
	400 °C + 600 °C[a]	t-ZrO_2 (0.73) + m-ZrO_2 (0.27)	14.5	14.4
	400 °C + 800 °C	m-ZrO_2 (0.67) + t-ZrO_2 (0.33)	15.6	15.6
	400 °C + 800 °C[a]	m-ZrO_2 (0.61) + t-ZrO_2 (0.39)	23.6	20.0
	400 °C + 500 MPa	m-ZrO_2 (0.67) + t-ZrO_2 (0.33)	8.8	7.6
	400 °C + 1000 MPa	m-ZrO_2 (0.71) + t-ZrO_2 (0.29)	8.3	7.6
	400 °C + 1350 MPa	m-ZrO_2 (0.83) + t-ZrO_2 (0.17)	8.0	7.5
Z9	–	amorphous	–	–
	400 °C	t-ZrO_2 (0.83) + m-ZrO_2 (0.17)	20.1	10.6
	400 °C + 600 °C	m-ZrO_2 (0.56) + t-ZrO_2 (0.44)	20.4	16.2
	400 °C + 800 °C	m-ZrO_2 (0.93) + t-ZrO_2 (0.07)	20.0	22.2
	400 °C + 500 MPa	m-ZrO_2 (0.59) + t-ZrO_2 (0.41)	18.9	11.1

continued

TABLE VII (cont.)

Sample	Treatment	Phase composition (volume fractions)	D_{hkl}/ nm	
			t-ZrO_2	m-ZrO_2
	400 °C + 1000 MPa	m-ZrO_2 (0.64) + t-ZrO_2 (0.36)	16.7	13.8
	400 °C + 1350 MPa	m-ZrO_2 (0.71) + t-ZrO_2 (0.29)	16.7	12.8
Z10	–	amorphous	–	–
	400 °C	t-ZrO_2	10.8	–
	400 °C + 600 °C	t-ZrO_2	12.3	–
	400 °C + 800 °C	t-ZrO_2 (0.97) + m-ZrO_2 (0.03)	17.7	–
	400 °C + 500 MPa	t-ZrO_2 (0.90) + m-ZrO_2 (0.10)	10.1	8.7
	400 °C + 1350 MPa	t-ZrO_2 (0.63) + m-ZrO_2 (0.37)	8.7	7.0
Z11	–	amorphous	–	–
	400 °C	t-ZrO_2	12.3	–
	400 °C + 600 °C	t-ZrO_2	14.3	–
	400 °C + 800 °C	t-ZrO_2 (0.97) + m-ZrO_2 (0.03)	19.7	–
	400 °C + 1350 MPa	t-ZrO_2 (0.89) + m-ZrO_2 (0.11)	12.3	11.7
Z12	–	amorphous	–	–
	400 °C	c-ZrO_2 + amorphous	6.6	–
	400 °C + 600 °C	t-ZrO_2	13.3	–
	400 °C + 800 °C	m-ZrO_2 (0.86) + t-ZrO_2 (0.14)	33.8	70.7
	400 °C + 1350 MPa	c- or t-ZrO_2 + amorphous	5.9	–
	600 °C + 1350 MPa	t-ZrO_2	12.9	–
	400 °C + 1350 MPa	m-ZrO_2 (0.72) + t-ZrO_2 (0.28)	15.3	10.4

[a]Before being subjected to the influence of temperature and pressure, samples were crashed in an agate mortar for 2 minutes.

The most susceptible t-ZrO_2 products to the influence of temperature were obtained at processing pH values between 6 and 8.[74–78] However, the temperature stability of t-ZrO_2 could not be attributed to the influence of pH value alone. In the presence of NO_3^- anions, the temperature stability of t-ZrO_2 increased with the decrease in pH, but in the presence of Cl^- anions, the pH value had little influence on the temperature stability.[78] The results of DSC and TG analysis showed that the nitrate content, incorporated into hydrous zirconia samples, decreased with the increase in pH. In sample Z7, prepared from suspensions with a high content of NO_3^- anions at pH = 7.5, the content of the present nitrate was very small and the obtained t-ZrO_2

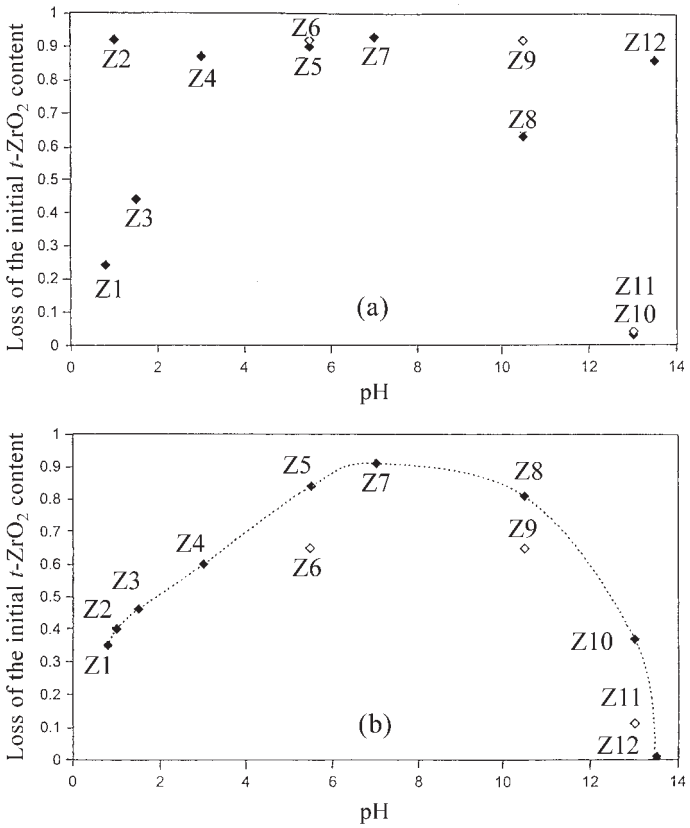

Figure 6. Loss of the initial t-ZrO_2 content (400 °C) on calcination at 800 °C (a) and pressure treatment at 1350 MPa (b) as a function of pH. Full and empty symbols represent the samples obtained by the hydrolytic polycondensation reaction at 100 °C and 25 °C, respectively.

proved to be the most susceptible. These results indicate that the temperature stability of a metastable t-ZrO_2 depends on the nitrate content in hydrous zirconia, while pH is just a mediator that provides a higher nitrate content in the obtained samples. Similarly, the adsorption of SO_4^{2-} anions caused an increase in the crystallization temperature of hydrous zirconia and an increase in the t-$ZrO_2 \rightarrow m$-ZrO_2 transformation by ≈200 °C.[74]

The obtained results show that the processing parameters, used to obtain hydrous zirconia, strongly influence the specific surface area, crystallite size and lattice strains of its crystallization products. There was a claim that these factors can stabilize the low-temperature t-ZrO_2.[5–8,10–16] Mitsuhashi *et al.*[15] found that the t-$ZrO_2 \rightarrow m$-ZrO_2 transformation occurred much

more easily in the strain-free t-ZrO_2 crystallite than in those with large strains. On the basis of these results, the authors concluded that lattice strains stabilized the low-temperature t-ZrO_2. Our results showed that lattice strains of t-ZrO_2 products increased almost linearly with an increase in pH (Figure 7). However, the stability of the corresponding t-ZrO_2 products did not follow this linear trend. The t-ZrO_2 in the crystallization products of samples obtained at a very low pH showed to be almost strain-free, but their stability was relatively high.

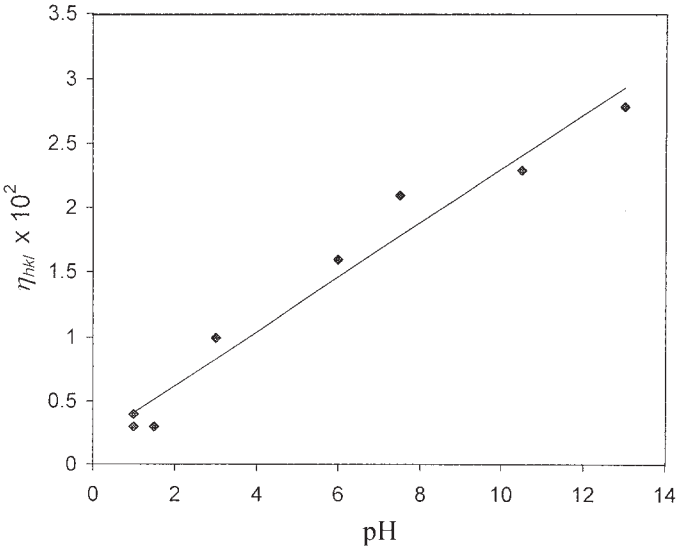

Figure 7. Influence of the processing pH on the lattice strain (η_{hkl}) of the crystallization products (400 °C) of the samples prepared by hydrolytic polycondensation at 100 °C.

The stabilizing influence of crystallite size, first suggested by Garvie,[10–12] was based on the assumption that surface energy factors could inhibit the t-$ZrO_2 \rightarrow m$-ZrO_2 transformation. Garvie proposed the critical crystallite size (≈30 nm) as the size limit below which t-ZrO_2 crystallites become thermodynamically more stable than m-ZrO_2 crystallites. The estimated crystallite sizes of t-ZrO_2 and m-ZrO_2 in the obtained crystallization products were much smaller than the proposed critical crystallite size (Table VII). However, most crystallization products contained bigger t-ZrO_2 crystallites than those of m-ZrO_2. Temperature treatment of the crystallization products caused an increase in the crystallite size followed by the t-$ZrO_2 \rightarrow m$-ZrO_2 transformation. On the other hand, pressure treatment caused a de-

crease in the crystallite sizes, which was also followed by the t-$ZrO_2 \rightarrow m$-ZrO_2 transformation. It was found that the crystallite sizes of t-ZrO_2 and m-ZrO_2 depended on the reaction temperature used to obtain hydrous zirconia. The hydrous zirconia samples obtained from the reaction mixture at RT yielded crystallization products with bigger t-ZrO_2 crystallites, while their stability increased under the influence of pressure (Figure 6). Similarly, the grinding of hydrous zirconia caused an increase in both the crystallite sizes and t-ZrO_2 content (Table VII). These results indicate that the crystallite size of metastable t-ZrO_2 is not the most important factor of its stabilization.

Srinivasan *et al.*[6,7] suggested that the surface sites adsorbing oxygen are responsible for the t-$ZrO_2 \rightarrow m$-ZrO_2 transformation. Covering of these sites with a substance such as SO_4^{2-} anions will prevent transformation and cause stabilization of the metastable t-ZrO_2. This conclusion also indicates that the samples with a smaller specific surface area will yield a more stable t-ZrO_2 product due to the smaller number of oxygen-deficient surface sites.

The shape of the curve showing the dependence of a specific surface area (σ) of the hydrous zirconia, characterized using the BET analysis, on the processing pH (Figure 8) has a considerable similarity to the shape of the curve showing the influence of pH on the stability of the t-ZrO_2 products

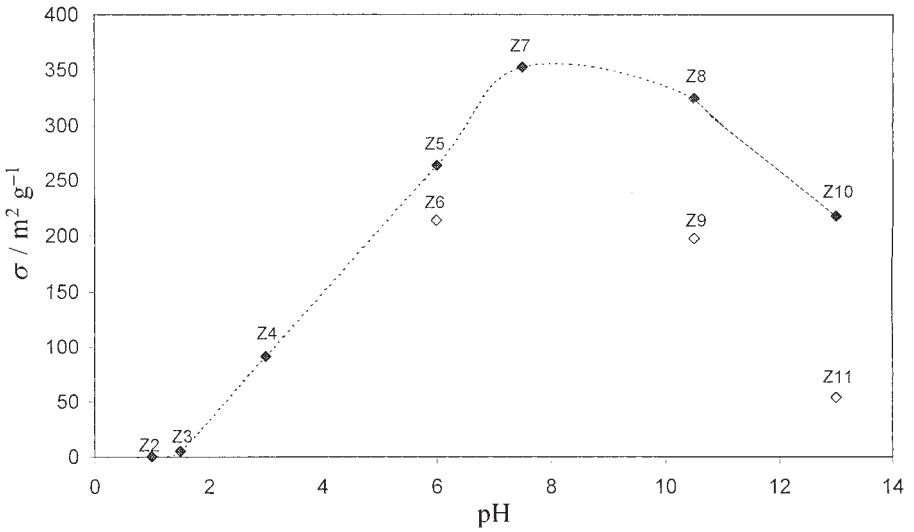

Figure 8. Influence of the processing pH on the specific surface area (σ) of the hydrous zirconia samples. Full and empty symbols represent the samples obtained by the hydrolytic polycondensation reaction at 100 °C and 25 °C, respectively.

subjected to pressure treatment (Figure 6). In all the examined samples, the hydrolytic polycondensation reaction at 100 °C caused an increase in the σ value followed by a decrease in the stability of the t-ZrO_2 products. The samples obtained from the suspensions at pH between 6 and 10.5 have the highest σ value and yield the most susceptible t-ZrO_2 products. However, the samples obtained from highly alkaline suspensions (pH $\geq$ 13) yield the most stable t-ZrO_2 products regardless of their relatively high σ values. The obtained results indicate that the specific surface area has some influence on the stability of t-ZrO_2 products, but it is not the only factor of stabilization. It can be concluded that the observed differences in t-ZrO_2 stability resulted from combined influences of several factors.

STABILIZATION IN THE ZrO_2–M_2O_3 SYSTEMS, M = Al, Fe, Cr

The tetragonal and cubic polymorphs of zirconia can be stabilized at RT by addition of suitable oxides, *viz.* MgO, CaO, Sc_2O_3, Y_2O_3, *etc.* Stabilization of the high-temperature polymorphs of ZrO_2 in these solid solutions was attributed to the decrease in the coordination number of the Zr^{4+} ion caused by incorporation of aliovalent dopant cations.[79] Li *et al.*[80] found that after calcination at 1300 °C, only oversized dopants could stabilize c-ZrO_2-type structures at RT. This stabilization was attributed to the decrease in the Zr coordination number by the introduction of oxygen vacancies associated with a smaller Zr cation. Incorporation of aliovalent undersized dopants also introduced oxygen vacancies, but the decrease in the Zr coordination number was smaller due to the association of the vacancies with the dopant cation.[80]

The cubic polymorph of zirconia could be partially stabilized by the incorporation of Fe^{3+} and Cr^{3+} ions.[78–82] The stabilization depends on both the amount of incorporated ions and the preparation conditions used.[80,81] Davidson *et al.*[82] and Berry *et al.*[83] found that c-ZrO_2 became stable in a sample with a Fe_2O_3 content higher than 20% (mole fraction, x). Hirano *et al.*[84] obtained similar results for the ZrO_2–Cr_2O_3 system. As a result of heating between 600 and 900 °C, the amorphous precursors of the ZrO_2–Cr_2O_3 system crystallized as metastable t-ZrO_2 (molar fraction of Cr_2O_3 less than 11%) or metastable c-ZrO_2 (Cr_2O_3 mole fraction between 11 and 20%).[84] On the other hand, Inwang *et al.*[85] concluded that, regardless of the iron content, stabilization of metastable c- or t-ZrO_2 depended on the processing pH value. Acid suspensions yield a crystallization product structurally closely related to t-ZrO_2, while alkaline suspensions give a crystallization product structurally closely related to c-ZrO_2.[85]

The capability of Al^{3+} ions to stabilize the cubic polymorph of zirconia is still a matter of discussion.[86–91] Several authors reported that the amorphous precursors to the ZrO_2–Al_2O_3 system crystallized after heating between 500 and 900 °C to a *c*-ZrO_2-type solid solution containing up to 40% (*x*) Al_2O_3.[86–88] At higher temperature, *c*-ZrO_2 converted to *t*-ZrO_2 and finally to *m*-ZrO_2 which was followed by a decrease in Al_2O_3 solubility. On the other hand, other reports[89–91] stated that the incorporation of Al^{3+} ions into ZrO_2 lattice stabilized only the tetragonal polymorph of zirconia. Balmer *et al.*[90,91] proposed the following phase evolution and partitioning in the ZrO_2–Al_2O_3 system during pyrolysis:

$$\text{amorphous} \rightarrow t\text{-}(\text{Zr, Al})\text{O}_2 \rightarrow t\text{-}(\text{Zr, Al})\text{O}_2 + \gamma\text{-}(\text{Al, Zr})_2\text{O}_3\,,$$
$$\downarrow \qquad\qquad \downarrow$$
$$m\text{-}\text{ZrO}_2 \qquad \alpha\text{-}\text{Al}_2\text{O}_3\,.$$

Thermodynamically Stable ZrO_2–M_2O_3 Systems

In the following investigations we examined phase compositions and solid solubility limits in the thermodynamically stable ZrO_2–M_2O_3 systems prepared using chemical coprecipitation and ceramic sintering.[92–94] The results of phase analysis showed that the solubility of Al^{3+} and Fe^{3+} ions in these systems is too small to stabilize high-temperature polymorphs of ZrO_2 (Table VIII). The results of the phase analysis of the ZrO_2–Fe_2O_3 system, obtained after calcination and cooling from 1100 °C in the presence of air at atmospheric pressure, show that in the whole concentration range there are two types of solid solutions, Z and F, structurally very closely related to *m*-ZrO_2 and α-Fe_2O_3, respectively.[92] The terminal solid solubility limits at RT, (2.0 ± 0.3)% of α-Fe_2O_3 in *m*-ZrO_2 and (1.0 ± 0.3)% of *m*-ZrO_2 in α-Fe_2O_3 (mole fractions, *x*), were estimated from the dependence of diffraction line intensities of both Z and F phases on the initial content of ZrO_2 and Fe_2O_3 and by extrapolation to zero intensity.

Similar results were obtained for the ZrO_2–Al_2O_3 system.[93] With the exception of the very ends of the concentration range, there are two types of solid solutions structurally very closely related to *m*-ZrO_2 and α-Al_2O_3. The terminal solid solubility limit of α-Al_2O_3 in *m*-ZrO_2 was estimated at (0.7 ± 0.3)%, while the solubility of *m*-ZrO_2 in α-Al_2O_3 was negligible.

The results of the ZrO_2–Cr_2O_3 system phase analysis showed that, regardless of the negligible solubility of Cr_2O_3 in ZrO_2, partial stabilization of a metastable *t*-ZrO_2 occurred.[94] Except for the very ends of the concentration range, identified as pure *m*-ZrO_2 and Cr_2O_3, the ZrO_2–Cr_2O_3 system contained the phases Cr_2O_3, *m*-ZrO_2 and metastable *t*-ZrO_2. The fraction of

TABLE VIII

The initial composition and the results of XRD phase analysis of the thermodynamically stable ZrO_2–M_2O_3 system. Phases Z, A and F are closely structurally related to *m*-ZrO_2, α-Al_2O_3 and α-Fe_2O_3, respectively

Mole fractions of M_2O_3	Phase compositions (relative fractions of ZrO_2 phases)		
	M = Al	M = Fe	M = Cr
–	*m*-ZrO_2	*m*-ZrO_2	*m*-ZrO_2
0.005	Z	Z	*m*-ZrO_2 (0.96) + *t*-ZrO_2 (0.04) + Cr_2O_3
0.015	Z+A	Z	*m*-ZrO_2 (0.96) + *t*-ZrO_2 (0.04) + Cr_2O_3
0.030	Z+A	Z+F	*m*-ZrO_2 (0.96) + *t*-ZrO_2 (0.04) + Cr_2O_3
0.050	Z+A	Z+F	*m*-ZrO_2 (0.96) + *t*-ZrO_2 (0.04) + Cr_2O_3
0.100	Z+A	Z+F	*m*-ZrO_2 (0.94) + *t*-ZrO_2 (0.06) + Cr_2O_3
0.200	Z+A	Z+F	*m*-ZrO_2 (0.88) + *t*-ZrO_2 (0.12) + Cr_2O_3
0.400	Z+A	Z+F	–
0.500	–	–	Cr_2O_3 + *m*-ZrO_2 (0.69) + *t*-ZrO_2 (0.31)
0.600	A+Z	F+Z	–
0.800	A+Z	F+Z	Cr_2O_3 + *m*-ZrO_2 (0.61) + *t*-ZrO_2 (0.39)
0.900	A+Z	F+Z	Cr_2O_3 + *m*-ZrO_2 (0.58) + *t*-ZrO_2 (0.42)
0.950	A+Z	F+Z	Cr_2O_3 + *m*-ZrO_2 (0.57) + *t*-ZrO_2 (0.43)
0.970	A+Z	F+Z	Cr_2O_3 + *m*-ZrO_2 + *t*-ZrO_2
0.985	A+Z	F+Z	Cr_2O_3 + *m*-ZrO_2 + *t*-ZrO_2
0.995	A+Z	F	Cr_2O_3 + *m*-ZrO_2 + *t*-ZrO_2
1	α-Al_2O_3	α-Fe_2O_3	Cr_2O_3

the *t*-ZrO_2 phase in the total content of ZrO_2 (*m*-ZrO_2 + *t*-ZrO_2) increased with an increase in the initial content of Cr_2O_3 (Figure 9).

The observed stabilization of metastable *t*-ZrO_2 could not be attributed to the formation of a solid solution. The stabilizing influence of Cr_2O_3 might be similar to the stabilizing influence of SO_4^{2-} anions, adsorbed onto the surface of ZrO_2 particles. Sohn *et al.*[95] showed that the influence of chromium oxides on the thermal behavior of amorphous zirconia was similar to the influence of SO_4^{2-} anions. The authors[95] concluded that the surface interaction between chromium oxides and ZrO_2 was very strong. This conclusion indicated that the stabilization of *t*-ZrO_2 in the presence of chromium oxide resulted from surface interaction. This interaction prevented the diffusion of oxygen from the atmosphere into the ZrO_2 lattice, which otherwise triggers the *t*-ZrO_2 → *m*-ZrO_2 transformation on cooling.

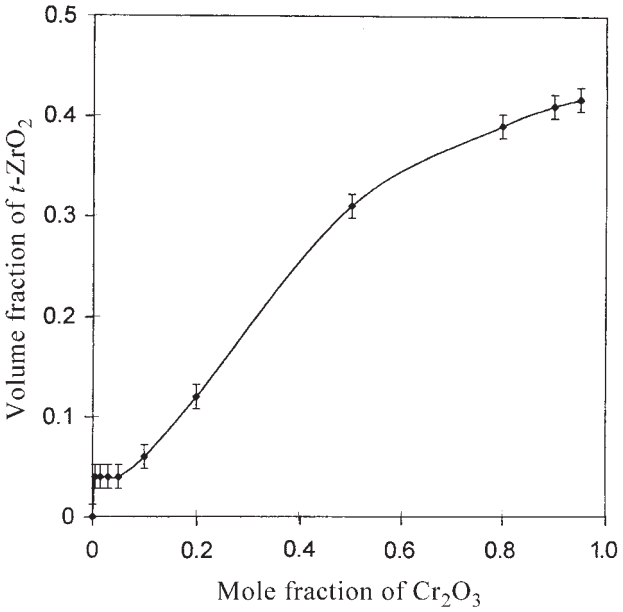

Figure 9. The t-ZrO_2 fraction in the total content of ZrO_2 (m-ZrO_2 + t-ZrO_2) as a function of the initial content of Cr_2O_3 (vertical bars represent the estimated experimental error). The samples from the ZrO_2–Cr_2O_3 system were prepared using chemical coprecipitation and ceramic sintering (maximum heating temperature was 1100 °C).

Metastable Phases in the ZrO_2–Fe_2O_3 and ZrO_2–Al_2O_3 Systems

Although the solubility of dopant cations in the thermodynamically stable ZrO_2–Fe_2O_3 and ZrO_2–Al_2O_3 systems was too small to stabilize high-temperature polymorphs of ZrO_2, it became significantly higher in the metastable solid solutions obtained after crystallization of amorphous precursors. In the following investigations, we examined the thermal behavior of these amorphous precursors.[81,96–98] The results of the DTA showed that the crystallization temperature of the amorphous precursors of the ZrO_2–Al_2O_3 system increased with an increase in the Al_2O_3 content from 405 °C for pure ZrO_2 to 915 °C for a sample with 60% (x) of Al^{3+} ions (Figure 10).[96] A similar result was observed for the ZrO_2–Fe_2O_3 system, but in that case the rate of the increase was lower (from 405 °C to 730 °C).[97] The observed increases indicated, in agreement with the results of Inwang *et al.*,[85] that amorphous precursors are single co-gels. Calcination of these amorphous precursors caused both crystallization and segregation in the starting phase. However, the activation energy required for the crystallization of amorphous precur-

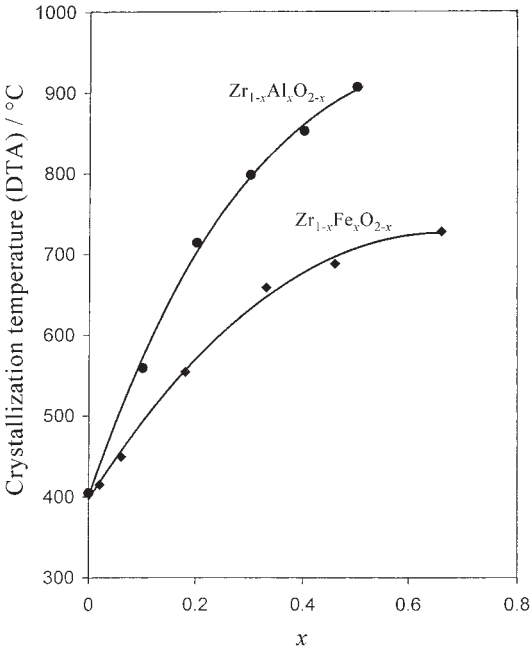

Figure 10. Effect of the dopant content (Fe^{3+} or Al^{3+} ions) on the temperature of the crystallization of the amorphous precursors to the ZrO_2–Fe_2O_3 and ZrO_2–Al_2O_3 systems.

sors is lower than the activation energy required for segregation in the starting phase. Due to this fact, the first crystallization product of amorphous precursors is a metastable phase with an extended capability for formation of solid solutions. Maximum solubility, obtained after crystallization of amorphous precursors, was estimated at ≈50% (x) of Fe^{3+} ions, while the solubility of Al^{3+} ions was even higher. Although the thermal behavior and maximum solubility showed to be very similar, the phase analysis results indicated that Al^{3+} and Fe^{3+} ions incorporated into ZrO_2 lattice in a different way. The phase analysis results obtained using both XRD and laser Raman spectroscopy showed that regardless of the very high solubility, Al^{3+} ions could not stabilize the cubic polymorph of ZrO_2 (Table IX). On the other hand, the incorporation of more than 10% of Fe_2O_3 stabilized the cubic polymorph of ZrO_2, while a smaller amount of Fe^{3+} ions stabilized tetragonal ZrO_2 (Table IX). In both systems, the increase of the temperature treatment caused a decrease of solid solubility limits, followed by a transformation into the monoclinic polymorph of ZrO_2. However, in the case of the ZrO_2–Fe_2O_3 system, this process occurred much faster.

TABLE IX

Phase development during the calcination of the amorphous precursors to the ZrO_2–M_2O_3 system in the presence of air at atmospheric pressure

$x(M^{3+})$	Temperature/°C	Phase composition (relative volume fractions of ZrO_2 phases)	
		M = Fe	M = Al
–	500	$Z_T(0.62) + Z_M(0.38)$	$Z_T(0.71) + Z_M(0.29)$
	600	$Z_M(0.85) + Z_T(0.15)$	$Z_M(0.63) + Z_T(0.37)$
	800	$Z_M(0.95) + Z_T(0.05)$	$Z_M(0.81) + Z_T(0.19)$
	1000	–	$Z_M(0.98) + Z_T(0.02)$
	1100	Z_M	Z_M
0.06	500	Z_T	–
	600	Z_T	–
	800	$Z_M(0.84) + Z_T(0.16)$	–
	1100	$Z_M + F$	–
0.10	500	–	Z_T
	600	–	Z_T
	800	–	Z_T
	1000	–	$Z_T(0.57) + Z_M(0.43)$
	1100	–	$Z_M(0.94) + Z_T(0.06)$
0.20	500	Z_C	Amorphous
	600	Z_C	Z_T
	800	$Z_T + F$	Z_T
	1000	–	Z_T
	1100	$Z_M + F$	$Z_M(0.93) + Z_T(0.07)$
0.30	600	Z_C	Amorphous
	800	$Z_T + F + Z_M$	Z_T
	1000	–	Z_T
	1100	$Z_M + F$	$Z_T + A$
0.40	600	Z_C	Amorphous
	700	–	Amorphous
	800	$Z_T + F + Z_M$	Z_T
	1000	–	Z_T
	1100	$Z_M + F$	$Z_T + A$

continued

TABLE IX (cont.)

$x(M^{3+})$	Temperature/°C	Phase composition (relative volume fractions of ZrO_2 phases)	
		M = Fe	M = Al
0.50	600	Z_C	Amorphous
	700	–	Amorphous
	800	$Z_T + F + Z_M$	Z_T
	1000	–	Z_T
	1100	$Z_M + F$	$Z_T + A$
0.65	600	$Z_C + F$	–
	800	$Z_T + F + Z_M$	Amorphous + A
	1000		$Z_T + A$
	1100	$Z_M + F$	$Z_T + A$

[a]Description: Z_M = phase structurally similar to *m*-ZrO_2, Z_T = phase structurally similar to *t*-ZrO_2, Z_C = phase structurally similar to *c*-ZrO_2, F = phase structurally similar to α-Fe_2O_3, A = phase structurally similar to δ-Al_2O_3.

Precise determination of unit-cell parameters of ZrO_2-type solid solutions from the ZrO_2–Fe_2O_3 and ZrO_2–Al_2O_3 systems, performed using the whole-powder-pattern decomposition method (Figure 11), are given in Table X. The unit-cell volume of both *t*- and *c*-ZrO_2-type solid solutions decreased linearly with the increase of the Fe_2O_3 content (Figure 12).

Kim *et al.*[99,100] proposed empirical equation that relates lattice constant of the *c*-ZrO_2-type solid solutions with the type (ionic radius, valency) and concentration of dopant cations. For the ZrO_2–$RO_{1.5}$ systems, this equation can be expressed as follows:

$$a_{Zr}/\text{nm} = 0.5120 + (0.0212\ \Delta r - 0.00022)m \tag{7}$$

where a_{Zr} is the lattice constant of the *c*-ZrO_2-type solid solutions, Δr is the difference in the ionic radius of dopant cation (R^{3+}) and the host cation (Zr^{4+}), and m is the concentration of the dopant cation (mole fraction/%) in the form of $RO_{1.5}$. When R = Fe, the equation (7) becomes:

$$a_{Zr}/\text{nm} = 0.5120 - 6.3 \times 10^{-4}\ m \tag{8}$$

The rate of the decrease obtained from our data showed to be somewhat smaller than it was expected by equation (8). The results of the regression

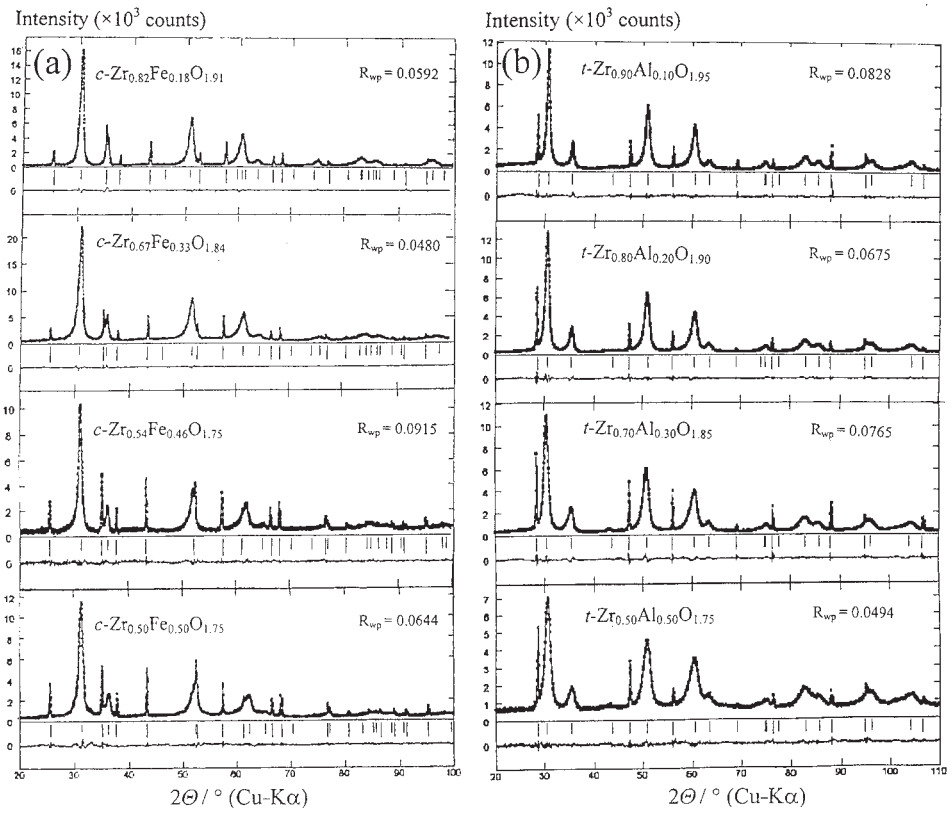

Figure 11. X-ray diffraction patterns of the c-ZrO_2-type solid solution from the ZrO_2–Fe_2O_3 system (a) and t-ZrO_2-type solid solution from the ZrO_2–Al_2O_3 system (b). Observed data are shown by squares, the refined pattern by full line. Positions of the diffraction lines of zirconia are shown by short, and those of internal standards by long bars. The difference, Δ, between the observed and refined patterns is also shown on the same scale in (a) and (b). Radiation Cu-Kα (40 kV, 30 mA).

analysis of our data give the following relation between the lattice constant (a_{Zr}) and the m value:

$$a_{Zr}/\text{nm} = 0.5125 - 3.6 \times 10^{-4}\, m \tag{9}$$

The transformation from the t-ZrO_2-type to c-ZrO_2-type solid solution has a very small influence on the unit-cell volume, probably because the coordination number of the Zr^{4+} ion (CN = 8) does not change in this transformation.

TABLE X

Refined values of unit-cell parameters of the *t*- or *c*-ZrO_2-type solid solutions with different amounts of incorporated Fe^{3+} or Al^{3+} ions

Phase	*a* / Å	*c* / Å	*V* / Å^3
t-ZrO_2	3.6057(6)	5.1475(14)	66.923
	5.0992[a]		133.846[a]
t-$Zr_{0.94}Fe_{0.06}O_{1.97}$	3.5919(3)	5.1596(8)	66.568
	5.0797[a]		133.136[a]
c-$Zr_{0.82}Fe_{0.18}O_{1.91}$	5.0643(3)		129.885
c-$Zr_{0.67}Fe_{0.33}O_{1.84}$	5.0138(4)		126.038
c-$Zr_{0.54}Fe_{0.46}O_{1.77}$	4.9591(7)		121.958
c-$Zr_{0.50}Fe_{0.50}O_{1.75}$	4.9380(8)		120.364
t-$Zr_{0.90}Al_{0.10}O_{1.95}$	3.5858(5)	5.0688(9)	65.174
	5.0711[a]		130.349[a]
t-$Zr_{0.80}Al_{0.20}O_{1.90}$	3.5828(4)	5.0633(6)	65.045
	5.0668[a]		129.987[a]
t-$Zr_{0.70}Al_{0.30}O_{1.85}$	3.5904(6)	5.0672(9)	65.321
	5.0776[a]		130.642[a]
t-$Zr_{0.60}Al_{0.40}O_{1.80}$	3.5836(5)	5.0637(8)	65.029
	5.0680[a]		130.058[a]
t-$Zr_{0.50}Al_{0.50}O_{1.75}$	3.5788(8)	5.0680(15)	64.910
	5.0612[a]		129.820[a]

[a]Related to fluorite type lattice.

Equation (7) predicts an even greater decrease of the unit-cell volume in the ZrO_2–Al_2O_3 system due to the smaller ionic radius of Al^{3+} ion (0.54 Å)[29] compared to Fe^{3+} ion (0.65 Å).[29] However, the increase of Al^{3+} content has a very small influence on the unit-cell volume of *t*-ZrO_2-type solid solutions (Table X). This result indicates that Al^{3+} ions incorporate into the ZrO_2 lattice interstitially.

Influence of Oxygen on the Phase Development in the ZrO_2–Fe_2O_3 System

The phase development during the calcination and cooling of the amorphous precursor to the ZrO_2–Fe_2O_3 system in the presence of air at atmospheric pressure (Table IX) was compared with the phase development during the calcination in vacuum ($\approx 4 \times 10^{-3}$ Pa) (Table XI). The obtained results indicated that the incorporation of Fe^{3+} cations stabilized the high tempera-

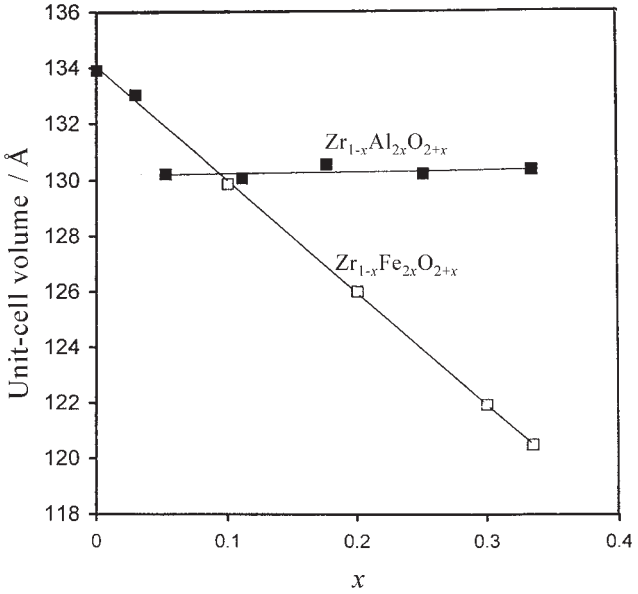

Figure 12. The influence of Fe_2O_3 and Al_2O_3 content on the unit-cell volume of t-ZrO_2- (■) and c-ZrO_2-type (□) solid solutions.

ture polymorphs of zirconia during calcination at standard air pressure but destabilized these polymorphs when calcinations were performed in vacuum. In order to explain these results, we must know the cause of stabilization of the high-temperature polymorphs of zirconia. In m-ZrO_2, the coordination number of the Zr^{4+} cation is 7, while in t- or c-ZrO_2 it is 8. The strongly covalent nature of the Zr–O bond favors the 7-fold coordination of zirconium and, therefore, only the monoclinic polymorph is thermodynamically stable at RT. However, the introduction of oxygen vacancies could stabilize high-temperature polymorphs, t-ZrO_2 (smaller amount of oxygen vacancies) or c-ZrO_2 (higher amount of oxygen vacancies), by reducing the coordination number of the Zr^{4+} cation. The usual way of introducing the oxygen vacancies into the ZrO_2 lattice is to form a solid solution with aliovalent oxides. Due to this fact, the presence of Fe^{3+} cations stabilizes the high temperature polymorphs during the calcination at standard air pressure. The lowest amount of oxygen vacancies required for stabilization of c-ZrO_2 was estimated at ≈6.5%,[79] assuming that all vacancies are associated with the Zr^{4+} cation. However, as shown in the work of Li *et al.*,[80] this will only occur when the dopant cations are of a significantly larger ionic size than the Zr^{4+} cation. On the other hand, if the dopant cations have a smaller ionic size, as in the case of Fe^{3+} cations, it is more likely that vacancies will be associated

TABLE XI

Results of the *in situ* phase analysis during the calcination of the samples at low air pressure ($\approx 4 \times 10^{-3}$ Pa)

Mole fraction of Fe_2O_3	Temperature/ °C	Phase composition
–	600	Amorphous + *c*-ZrO_2
	800	*c*-ZrO_2
	1000	*c*-ZrO_2
	1200	*c*-ZrO_2 + *t*-ZrO_2
0.01	600	Amorphous + Z_C
	800	Z_C
	1000	$Z_C + Z_M$
	1200	$Z_C + Z_M$
0.03	600	Amorphous + Z_C
	800	Z_C
	1000	$Z_C + Z_M$
	1200	$Z_C + Z_M$
0.10	600	Amorphous + Z_C
	800	Z_C
	1000	$Z_C + Z_M$
	1200	$Z_M + Z_C$
0.20	600	Amorphous + Z_C
	800	Z_C
	1000	$Z_M + Z_C + Z_T + F_M$
	1200	$Z_M + Z_T + F_M$
0.30	600	Amorphous + Z_C
	800	$Z_C + F_H$
	900	$Z_C + Z_M + F_H$
	1000	$Z_C + Z_M + H + F_M$
	1200	$Z_M + Z_C + H + F_M$
0.50	600	Amorphous + F_H
	800	$Z_C + F_H$
	1000	$Z_C + F_H + Z_M$
	1200	$F_H + Z_C + Z_M$

[a]Z_M, Z_C, Z_T, F_H and F_M are phases structurally closely related to *m*-ZrO_2, *c*-ZrO_2, *t*-ZrO_2, α-Fe_2O_3 and Fe_3O_4, respectively.

with them. In our work,[98] oxygen vacancies are introduced into the ZrO_2 lattice as a result of calcination at low pressure. The presence of these vacancies stabilizes the *c*-ZrO_2 in the sample with $x(Fe_2O_3) = 0$. Introduced vacancies tend to associate with smaller dopant cations such as Fe^{3+}. Possibly, due to this fact, the presence of iron destabilizes the high temperature polymorphs of zirconia and causes the appearance of monoclinic and tetragonal phases (Figure 13).

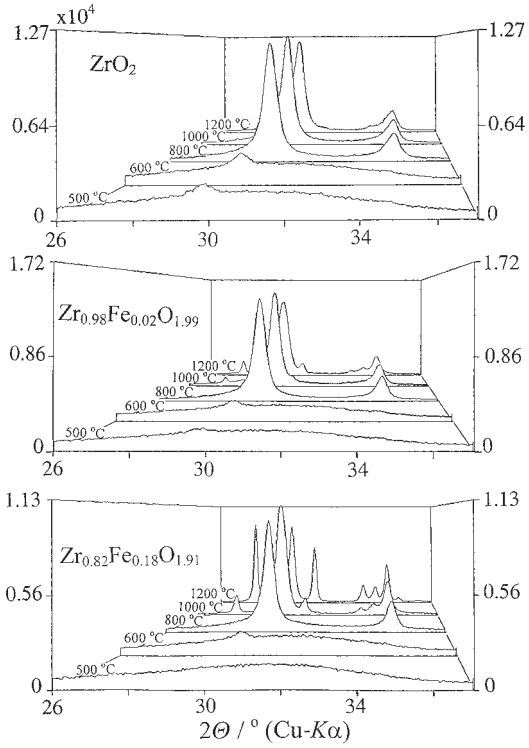

Figure 13. Characteristic parts of the X-ray diffraction patterns obtained during calcinations of the amorphous precursors to ZrO_2, $Zr_{1.98}Fe_{0.02}O_{1.99}$ and $Zr_{0.82}Fe_{0.18}O_{1.91}$ at low air pressure ($\approx 4 \times 10^{-3}$ Pa).

REFERENCES

1. R. Stevens, *Zirconia and Zirconia Ceramics*, Magnesium Electron Ltd., Publication No. 113, July 1986, Litko 2000, Twickenham, U.K.
2. I. Clark and D. H. Reynolds, *Ind. Eng. Chem*. **29** (1937) 711–715.

3. B. C. Weber and M. A. Schwartz, *Ber. Dtsch. Keram. Ges.* **34** (1957) 391–414.
4. R. Cypres, R. Wollast, and J. Raucq, *Ber. Dtsch. Keram. Ges.* **40** (1963) 527–532.
5. R. Srinivasan, D. Taulbee, and B. H. Davis, *Catal. Lett*. **9** (1991) 1–8.
6. R. Srinivasan, T. R. Watkins, C. R. Hubbard, and B. H. Davis, *Chem. Mater.* **7** (1995) 725–730.
7. S. Chokkaram, R. Srinivasan, D. R. Milburn, and B. H. Davis, *J. Colloid Interface Sci.* **165** (1995) 160–168.
8. F.-C. Wu and S.-C. Yu, *J. Mater. Sci*. **25** (1990) 970–976.
9. K. M. Parida and P. K. Pattnayak, *J. Colloid Interface Sci.* **182** (1996) 381–387.
10. R. C. Garvie, *J. Phys. Chem*. **69** (1965) 1238–1243.
11. R. C. Garvie, *J. Phys. Chem*. **82** (1978) 218–224.
12. R. C. Garvie and M. F. Goss, *J. Mater Sci*. **21** (1986) 1253–1257.
13. E. Bailey, D. Lewis, Z. M. Librant, and L. J. Porter, *Trans. J. Br. Ceram. Soc.* **71** (1972) 25–30.
14. A. N. Scian, E. F. Aglietti, M. C. Caracohe, P. C. Rivas, A. F. Pasquevich and A. R. L. Garcia, *J. Am. Ceram. Soc*. **77** (1994) 1525–1530.
15. T. Mitsuhasi, M. Ichihara, and U. Tatsuke, *J. Am. Ceram. Soc*. **57** (1974) 97–101.
16. H.-C. Wang and K.-L. Lin, *J. Mater. Sci.* **26** (1991) 2501–2506.
17. J. Livage, K. Doi, and C. Mazieres, *J. Am. Ceram. Soc*. **51** (1968) 349–353.
18. G. Keramidas and W. B. White, *J. Am. Ceram. Soc*. **57** (1974) 22–24.
19. E. Tani, M. Yoshimura, and S. Somiya, *J. Am. Ceram. Soc*. **66** (1983) 111–114.
20. M. A. Blesa, A. J. G. Maroto, S. I. Passaggio, N. E. Figliolia, and G. Rigotti, *J. Mater. Sci*. **20** (1985) 4601–4609.
21. R. P. Denkewicz, K. S. TenHuisen, and J. H. Adair, *J. Mater. Res*. **5** (1990) 2698–2705.
22. J. Torralvo, M. A. Alario, and J. Soria, *J. Catal.* **86** (1984) 473–476.
23. I. Osendi, I. S. Moya, C. I. Serna, and I. Soria, *J. Am. Ceram. Soc*. **68** (1985) 135–139.
24. Y. Murase and E. Kato, *J. Am. Ceram. Soc*. **66** (1983) 196–200.
25. Y. Murase and E. Kato, *J. Am. Ceram. Soc.,* **62** (1979) 527.
26. Y. Zeng, G. Fagherazzi, and S. Polizzi, *J. Mater. Sci.* **30** (1995) 2153–2158.
27. O. Stachs, Th. Gerber, and V. Petkov, *J. Non-Cryst. Solids* **210** (1997) 14–22.
28. H. Toraya, M. Yoshimura, and S. Somiya, *J. Am. Ceram. Soc*. **67** (1984) C119–C121.
29. H. P. Klug and L. E. Alexander, *X-ray Diffraction Procedures*, 2nd edition, John Wiley & Sons, New York 1974, pp. 640–642.
30. H. Toraya, *J. Appl. Cryst*. **19** (1986) 440–447.
31. H. Toraya, *J. Appl. Cryst*. **26** (1993) 583–590.
32. D. P. C. Thackeray, *Spectrochim. Acta* **30A** (1974) 549–550.
33. M. Ishigame and T. Sakurai, *J. Am. Ceram. Soc*. **60** (1977) 367–369.
34. H. Arashi and M. Ishigame, *Phys. Status Solidi* **71** (1982) 313–321.
35. D. R. Clarke and F. Adar, *J. Am. Ceram. Soc*. **65** (1982) 284–288.
36. C. H. Perry, F. Lu, D. W. Liu, and R. P. Ingel, *J. Am. Ceram. Soc*. **68** (1985) C–184–C–187.
37. C. H. Perry, F. Lu, D. W. Liu, and B. Alzyab, *J. Raman Spectrosc.* **21** (1990) 577–584.
38. K. Matsui, H. Suzuki, M. Ohgai, and H. Arashi, *J. Ceram. Soc. Jpn.* **98** (1990) 15–19.

39. K. Matsui, H. Suzuki, M. Ohgai, and H. Arashi, *J. Am. Ceram. Soc*. **78** (1995) 146–152.
40. D. J. Kim, H Jung, and I. S. Yang, *J. Am. Ceram. Soc*. **76** (1993) 2106–2108.
41. M. Yashima, K. Ohtake, H. Arashi, M. Kakihana, and M. Yoshimura, *J. Appl. Phys*. **74** (1993) 7603–7605.
42. M. Yashima, H. Arashi, M. Kakihana, and M. Yoshimura, *J. Am. Ceram. Soc*. **77** (1994) 1067–1071.
43. T. Hirata, *J. Phys. Chem. Solids* **56** (1995) 951–957.
44. R. Srinivasan, S. F. Simpson, J. M. Harris, and B. H. Davis, *J. Mater. Sci. Lett.,* **10** (1991) 352–354.
45. N. T. McDevitt and W. L. Baun, *J. Am. Ceram. Soc*. **47** (1964) 622–624.
46. C. M. Phillippi and K. S. Mazdiyasni, *J. Am. Ceram. Soc*. **54** (1971) 254–258.
47. D. M. Lui, C. H. Perry, and R. P. Ingel, *J. Appl. Phys.* **64** (1988) 1415–1417.
48. G. Štefanić, S. Musić, S. Popović, and K. Furić, *Croat. Chem. Acta* **69** (1996) 223–239.
49. T. Hirata, E. Asari, and M. Kitajima, *J. Solid State Chem*. **110** (1994) 201–207.
50. G. Štefanić, S. Musić, and S. Popović, *Thermochim. Acta* **259** (1995) 225–234.
51. V. V. Mishra, A. K. Garg, and D. C. Agrawal, *Bull. Mater. Sci*. **21** (1998) 81–86.
52. B. H. Davis, *J. Am. Ceram. Soc*. **67** (1984) C–168.
53. R. Srinivasan, M. B. Harris, S. F. Simpson, R. J. DeAngelis, and B. H. Davis , *J. Mater. Res*. **3** (1988) 787–797.
54. R. Srinivasan and B. H. Davis, *Catal. Lett*. **14** (1992) 165–170.
55. A. Clearfield, *J. Mater. Res*. **5** (1990) 161–162.
56. G. Štefanić, S. Musić, and A. Sekulić, *Thermochim. Acta* **273** (1996) 119–133.
57. S. Musić, G. Štefanić, N. Vidović, and A. Sekulić, *J. Therm. Anal. Cal.* **59** (2000) 837–846.
58. H. Sariçemen, *Powder Technol*. **27** (1980) 23–28.
59. P. E. Morgan, *J. Am. Ceram. Soc*. **67** (1984) C–204–C–205.
60. E. Tani, M. Yoshimura, and S. Somiya*, J. Am. Ceram. Soc*. **64** (1981) C–181.
61. H. Cheng , L. Wu, J. Ma, Z. Zhao, and L. Qi*, J. Mater. Sci. Lett*. **15** (1996) 895–897.
62. H. Nishizawa, N. Yamasaki, and K. Matsuoka, *J. Am. Ceram. Soc*. **65** (1982) 343–346.
63. G. Štefanić, S. Popović, and S. Musić, *Thermochim. Acta* **303** (1997) 31–39.
64. M. Bućko, K. Haberko, M. Faryna, *J. Am. Ceram. Soc*. **78** (1995) 3397–3400.
65. E. Kato, M. Hirano, and A. Nagi, *J. Am. Ceram. Soc*. **78** (1995) 2259–2262.
66. J. H. Adair, R. P. Denkewicz, F. J. Arrigada, and K. Ossero-Asare, *Ceram. Trans., Ceram. Powder Sci.* **1** (1988) 135–145.
67. A. Clearfield and P. A. Vaughan, *Acta Cryst*. **9** (1956) 555–558.
68. T. Mamott, P. Barnes, S. E. Tarling, S. L. Jones, and C. I. Norman, *J. Mater. Sci.* **26** (1991) 4054–4061.
69. R. Srinivasan, B. H. Davis, O. Burl Cavin, and C. R. Hubbard, *J. Am. Ceram Soc*. **75** (1992) 1217–1222.
70. R. Srinivasan, C. R. Hubbard, O. B. Cavin, and B. H. Davis, *Chem. Mater.* **5** (1993) 27–31.
71. G. Štefanić and S. Musić, unpublished results.
72. G. Štefanić, B. Gržeta, S. Popović, and S. Musić, *Croat. Chem. Acta* **72** (1999) 395–412.
73. R. C. Garvie, R. H. Hannink, and R. T. Pascoe, *Nature* **258** (1975) 703–704.

74. G. Štefanić, S. Musić, S. Popović, and A. Sekulić, *J. Mol. Struct*. **408/409** (1997) 391–394.
75. G. Štefanić, S. Musić, B. Gržeta, S. Popović, and A. Sekulić, *J. Phys. Chem. Solids* **59** (1998) 879–885.
76. G. Štefanić, S. Musić, B. Gržeta, S. Popović, and A. Sekulić, *Croat. Chem. Acta* **71** (1998) 789–806.
77. I. I. Štefanić, S. Musić, G. Štefanić, and A. Gajović, *J. Mol. Struct.* **480/481** (1999) 621–625.
78. G. Štefanić, I. I. Štefanić, and S. Musić, *Mater. Chem. Phys*. **65** (2000) 197–207.
79. S. M. Ho, *Mater. Sci. Eng*. **54** (1982) 23–29.
80. P. Li, I.-W. Chen, and J. E. Penner-Hahn, *J. Am. Ceram. Soc*. **77** (1994) 118–128.
81. G. Štefanić, S. Musić, S. Popović, and K. Nomura, *J. Mol. Struct.* **480/481** (1999) 627–631.
82. S. Davison, R. Kershaw, K. Dwight, and A. Wold, *J. Solid State Chem.* **73** (1988) 47–51.
83. F. j. Berry, M. H. Loretto, and M. R. Smith, *J. Solid State Chem*. **83** (1989) 91–99.
84. S. Hirano, M. Yoshinaka, K. Hirota, and O. Yamaguchi, *J. Am. Ceram. Soc*. **79** (1996) 171–176.
85. I. B. Inwang, F. Chyad, and I. J. McColm, *J. Mater. Chem*. **5** (1995) 1209–1213.
86. O. Yamaguchi, M. Shirai, and M. Yoshinaka, *J. Am. Ceram. Soc*. **71** (1988) C–510–C–512.
87. K. Ishida, K. Hirota, O. Yamaguchi, H. Kume, S. Inamura, and H. Miyamoto, *J. Am. Ceram. Soc.* **77** (1994) 1391–1395.
88. W. Zhang, E. E. lachowski, and F. P. Glasser, *J. Mater. Sci*. **28** (1993) 6222–6232.
89. S. Moreau, M. Gervais, and A. Douy, *Solid State Ionics* **101–103** (1997) 625–631.
90. M. L. Balmer, F. F. Lange, and C. G. Levi, *J. Am. Ceram. Soc*. **77** (1994) 2069–2075.
91. M. L. Balmer, F. F. Lange, V. Jayaram, and C. G. Levi, *J. Am. Ceram. Soc*. **78** (1995) 1489–1494.
92. S. Popović, B. Gržeta, G. Štefanić, I. Cakó-Nagy, and S. Musić, *J. Alloys Comp*. **241** (1996) 10–15.
93. S. Popović, G. Štefanić, and S. Musić, *Mater. Lett*. **31** (1997) 19–22.
94. G. Štefanić, S. Popović, and S. Musić, *Mater. Lett*. **36** (1998) 240–244.
95. J. R. Sohn, S. G. Ryu, M. Y. Park, and Y. I. Pae, *J. Mater. Sci*. **28** (1993) 4651–4659.
96. G. Štefanić and S. Musić, unpublished results.
97. G Štefanić, B. Gržeta, K. Nomura, R. Trojko, and S. Musić, *J. Alloys Comp*. **327** (2001) 151–160.
98. G. Štefanić, B. Gržeta, and S. Musić, *Mater. Chem. Phys.* **65** (2000) 216–221.
99. D.-J. Kim, *J. Am. Ceram. Soc*. **72** (1989) 1415–1421.
100. D.-J. Kim, S.-H. Hyun, S.-G. Kim, and M.Yashima, *J. Am. Ceram. Soc*. **77** (1994) 597–599.

SAŽETAK

Faktori koji utječu na stabilnost niskotemperaturnog tetragonskog ZrO_2

Goran Štefanić i Svetozar Musić

Pomno su istraživani različiti faktori koji utječu na javljanje tetragonskog (*t*-) polimorfa ZrO_2 pri sobnoj temperaturi. Nekoliko predloženih modela naglašava ulogu anionskih nečistoća (SO_4^{2-}, OH^-), veličine kristala (površinske energije), strukturne sličnosti između polaznog materijala i *t*-ZrO_2, napetosti u kristalnoj rešetki, vodene pare, defekata u kristalnoj rešetki (kisikovih vakancija), itd. Naša istraživanja, usredotočena na stabilnost niskotemperaturnog *t*-ZrO_2, pokazuju da bez obzira na strukturne razlike polaznih cirkonijskih materijala produkti njihove termičke razgradnje kristaliziraju u metastabilni *t*-ZrO_2. Prijelaz *t*-$ZrO_2 \rightarrow$ *m*-ZrO_2 javlja se za vrijeme hlađenja ili daljnjeg žarenja u prisutnosti zraka pri atmosferskom tlaku. S druge strane, ako se ti procesi provode u vakuumu metastabilna faza ostaje očuvana. Ta opažanja upućuju na to da se metastabilni *t*-ZrO_2 javlja pri sobnoj temperaturi uslijed stabilizacije uzrokovane uvođenjem kisikovih vakancija, slično kao i kod čvrstih otopina s kationima manje valencije. Smanjenje specifične površine zrnaca ZrO_2 ili prisutnost tvari koje imaju jake površinske interakcije sa ZrO_2 (SO_4^{2-}, Cr_2O_3) sprječava difuziju kisika iz atmosfere u kristalnu rešetku ZrO_2, te uslijed toga *t*-ZrO_2 biva stabiliziran. S druge strane, napetosti u kristalnoj rešetki i veličine zrnaca metastabilnog *t*-ZrO_2 ne mogu biti jasno povezane s njegovom stabilnošću.